Department of Chemistry
University of Helsinki
Finland

Phase behavior of poly(2-propyl-2-oxazoline)s

Fabian Pooch

ACADEMIC DISSERTATION

To be presented, with the permission of the Faculty of Science of the University of Helsinki, for public examination in lecture room A110, Chemicum, on 24 October 2019, at 12 noon.

Helsinki 2019

Supervisors

Prof. Heikki Tenhu and Prof. Francoise Winnik
Department of Chemistry
University of Helsinki
Finland

Opponent

Prof. Philippe Guégan
Parisian Institute for Molecular Chemistry
Sorbonne Université
France

Reviewers

Prof. Carl-Eric Wilén
Laboratory of Polymer Technology
Faculty of Science and Engineering
Åbo Akademi University
Finland

Prof. emeritus Helge Lemmetyinen
Docent in Physical Chemistry
University of Helsinki
Finland

ISBN 978-951-51-5510-8 (pbk.)
ISBN 978-951-51-5511-5 (PDF)

Helsinki University Printing House
Helsinki 2006

Abstract

Poly(2-oxazoline)s consist of a -(CH_2-CH_2-N)- main chain and an *N*-acyl substituent. They were reported for the first time in 1966/67. They have been investigated in the bulk, in solutions and in dispersions. The recent interest lies primarily in their chemical versatility and their potential for nanomedical applications. Tailoring materials for such specific applications requires a sound knowledge of their phase behaviors, which depends on intensive parameters. Amongst others, composition and temperature are of particular interest. The phase behaviors of poly(2-propyl-2-oxazoline)s (PPOxs) will be the main focus of this thesis. PPOx homopolymers are investigated as well as block copolymers (BCPs) and blends of poly(2-isopropyl-2-oxazoline) (PiPOx) and poly(lactide) (PLA).

The first part describes the synthesis of the polymers. The PPOxs are prepared by cationic ring opening polymerization. They are linear, narrowly dispersed, and bear at the termini one methyl- and one azide-group. Semi-crystalline as well as amorphous PLA is synthesized by ring opening polymerization of *L*-lactide and *DL*-lactide, respectively. The linear PLAs are terminated with one propargyl- and one hydroxyl-group. Coupling of the azido- and alkyne-functional homopolymers gives a library of 18 PiPOx-*b*-PLA BCPs. This approach allows to compare the phase behaviors of the BCPs with those of the individual components.

The next part is dedicated to a study of the solution properties of three PPOx homopolymers, namely poly(2-n-propyl-2-oxazoline) (PnPOx), poly(2-cyclopropyl-2-oxazoline) (PcyPOx) and PiPOx in water, in methanol and in water/methanol mixtures. Nuclear magnetic resonance (NMR) spectroscopy of the three polymers reveals significant differences in the side-group's rotational freedom. Unexpectedly, these differences are reflected in the calorimetric assessment of the coil-to-globule phase transition. The phase diagrams in respect to the water/methanol composition are constructed based on transmittance measurements. Methanol is a good solvent up to its boiling point for the three PPOxs. The solubility of PnPOx in water decreases when up to 40 vol% methanol is added. This behavior termed "cononsolvency" was first reported for ternary polymer/water/methanol mixtures of poly(*N*-isopropyl acrylamide), a structural isomer of PnPOx and PiPOx. PiPOx and PcyPOx do not exhibit cononsolvency in the investigated ternary system. The PPOxs' solution behaviors depend on the rotational freedom of the side-groups.

In the third part, the bulk phase behavior of PiPOx, its blends with PLA, and PiPOx-*b*-PLA BCPs is studied. The PiPOx volume fractions in the BCPs varies from 14 to 82 %. PiPOx and PLA are miscible based on the single glass transition criterion and small angle x-ray scattering at a temperature above the melting points of the two polymers. Infrared spectroscopy indicates an attractive dipole-dipole interaction between the carbonyl moieties of the PiPOx amide and the carbonyl of the PLA ester. PiPOx and the stereo-regular PLLA are semi-crystalline. The influence of the miscibility on the crystallization is investigated by polarized optical microscopy, differential scanning calorimetry and wide-angle x-ray scattering. It is found that the presence of PLA increases the crystallization rate of PiPOx. In contrast, PLLA remains amorphous in most of the BCPs.

The last part focuses on aqueous dispersions of the self-assembled PiPOx-*b*-PLA BCPs. The dispersions were prepared by adding a solution of a BCP in THF to water, a non-solvent of PLA but a solvent of PiPOx at low temperature. Contrary to expectation PiPOx resides in the particle interior, together with PLA. It does not form a shell of hydrated chains around the PLA core. This conclusion was attained on the basis of NMR spectroscopy and evaluation of the thermo-responsive properties of the BCP particle dispersions in water. At room temperature the particles are colloidally stable for 20 days at least. The particle morphology is investigated by cryogenic transmission electron microscopy, light scattering and small angle neutron scattering. The particles are spherical and permeated with water over the wide PiPOx volume fraction. Short segments of PiPOx reside on the particle/water interface and stabilize the dispersion. The thermo-responsive properties of the dispersions depend on the configuration and length of these segments. Attractive interactions between soluble and insoluble block are an important factor for the self-assembly of amphiphilic BCPs.

Acknowledgements

This work was conducted in the years 2013 - 2019 at the Department of Chemistry, University of Helsinki and was funded by Tekes and the University of Helsinki.

I wish to express my deepest gratitude to my supervisors Prof. Heikki Tenhu and Prof. Francoise Winnik for enabling this work. Through the years I experienced always your encouragement and support. Thank you also for editing my texts and eliminating most of my Germanisms, though I fear they will continue to come through every now and then. Through your dedication I learned how to compose a scientific article.

My collaborators Prof. Bo Nyström, Dr. Kenneth Knudsen, Dr. Kirsi Svedström, Dr. Erno Karjalainen, Marjolein Sliepen, Antti Korpi, and Valerij Teltevskij are gratefully acknowledged. Thank you for your input and support.

I wish to thank Prof. Carl-Eric Wilén and Prof. Helge Lemmetyinen for examining my thesis and Prof. Philippe Guégan for traveling to Helsinki to be my opponent.

I am grateful to Prof. Sirkka Maunu for leading our group. Special thanks to Seija Lemettinen, Juha Solasaari, Dr. Vladimir Aseyev, Dr. Sami Hietala, Dr. Sami-Pekka Hirvonen and Ennio Zuccaro for their excellent support through the years. Thank you to all my colleagues for creating a great atmosphere in the group. I will always remember our conference trips, our futsal and floorball games, and many other activities.

Meiner und Tinas Familie möchte ich von tiefstem Herzen meinen Dank aussprechen. Auch wenn der persönliche Kontakt in den letzten Jahren wenig regelmäßig war, so wart ihr doch jeden Tag bei mir.

Zu guter Letzt bedanke ich mich bei der Frau meines Lebens, Tina, für deinen Zuspruch, deine Begeisterung und deinen Enthusiasmus in jeder Situation. Dein Einfluss auf diese Arbeit kann nicht gemessen werden. Ich freue mich auf viele weitere Tage mit dir.

Contents

List of original publications

This thesis is based on the following publications:

I Pooch, F.; Teltevskij, V.; Karjalainen, E.; Tenhu, H.; Winnik, F. M. **Poly(2-propyl-2-oxazoline)s in aqueous methanol: to dissolve or not to dissolve….** *Macromolecules*, **2019,** *52*, 6361-6368. DOI: 10.1021/acs.macromol.9b01234

II Pooch, F.; Sliepen, M.; Svedström, K. J.; Korpi, A.; Winnik, F. M.; Tenhu, H. **Inversion of crystallization rates in miscible block copolymers of poly(lactide)-*block*-poly(2-isopropyl-2-oxazoline).** *Polymer Chemistry* **2018**, *9*, 1848-1856. DOI: 10.1039/c8py00198g

III Pooch, F.; Sliepen, M.; Knudsen, K. D.; Nyström, B.; Tenhu, H.; Winnik, F. M. **Poly(2-isopropyl-2-oxazoline)-*b*-poly(lactide) (PiPOx-*b*-PLA) Nanoparticles in Water: Interblock van der Waals Attraction Opposes Amphiphilic Phase Separation.** *Macromolecules* **2019**, *52*, 1317-1326. DOI: 10.1021/acs.macromol.8b02558

The publications are referred to in the text by their roman numerals.

The author's contribution to the publications:
For the three publications F. Pooch drafted the research plan, designed the experiments and conducted most of the synthesis and characterization. Pooch wrote the first draft of the manuscripts and finalized them with the coauthors.

Abbreviations

ATR	attenuated total reflection
BCP	block copolymer
$CDCl_3$	deuterated chloroform
CROP	cationic ring opening polymerization
Cryo-TEM	cryogenic transmission electron microscopy
cyPOx	2-cyclopropyl-2-oxazoline
D	diffusion coefficient
D_2O	deuterium oxide
DLS	dynamic light scattering
DMAc	*N*,*N*-dimethyl acetamide
DMF	*N*,*N*-dimethyl formamide
DOSY	diffusion ordered spectroscopy
DP	degree of polymerization
DSC	differential scanning calorimetry
FT-IR	Fourier transform infrared spectroscopy
FWHM	full width at half maximum
H-bond	hydrogen bond
iPOx	2-isopropyl-2-oxazoline
LCST	lower critical solution temperature
MALDI ToF	matrix assisted laser desorption ionization time of flight mass spectrometry
M_n	number average molecular weight
M_w	weight average molecular weight
NMR	nuclear magnetic resonance spectroscopy
NOESY	Nuclear Overhauser Effect spectroscopy
nPOx	2-n-propyl-2-oxazoline
P(*q*)	form factor
PAA	poly(acrylic acid)
PcyPOx	poly(2-cyclopropyl-2-oxazoline)
PD	polydispersity
PDLLA	poly(*DL*-lactide)
PEG	poly(ethylene glycol)
PEG-*b*-PLA	poly(ethylene glycol)-*block*-poly(lactide)
PEtOx	poly(2-ethyl-2-oxazoline)
PiPOx	poly(2-isopropyl-2-oxazoline)
PiPOx-*b*-PLA	poly(2-isopropyl-2-oxazoline)-*block*-poly(lactide)
PLA	poly(lactide)
PLLA	poly(*L*-lactide)
THF	tetrahydrofuran
PMeOx	poly(2-methyl-2-oxazoline)
PNIPAM	poly(*N*-isopropyl acrylamide)
PnPOx	poly(2-n-propyl-2-oxazoline)

POM	polarized optical microscopy
PPOx	poly(2-propyl-2-oxazoline)
PVA	poly(vinyl alcohol)
PVC	poly(vinyl chloride)
PVPh	poly(vinyl phenol)
q	scattering vector
R	universal gas constant
R_g	radius of gyration
R_h	hydrodynamic radius
SANS	small angle neutron scattering
SAXS	small angle x-ray scattering
SEC	size exclusion chromatography
SLS	static light scattering
T	temperature
T_c	crystallization temperature
T_{CP}	cloud point temperature
T_g	glass transition temperature
T_m	melting temperature
$T_m°$	equilibrium melting temperature
T_{max}	temperature at the maximum of an endotherm
T_{trans}	transition temperature
UCST	upper critical solution temperature
v_A	molar volume of compound A
w_{AA}	pair interaction energy between two molecules of A
WAXS	wide angle x-ray scattering
x_A	mole fraction of compound A
X_p	monomer conversion
z	coordination number
Γ	decay rate
δ_A	solubility parameter of compound A
$\Delta_M G$	free energy of mixing
$\Delta_M H$	enthalpy of mixing
$\Delta_M S$	entropy of mixing
ΔT	degree of undercooling
µDSC	high sensitivity differential scanning calorimetry
$\tau_{1/2}^{-1}$	inverse of the crystallization half time
υ	reference volume
ϕ_A	volume fraction of compound A
χ_{AB}	Flory-Huggins parameter of compounds A and B

1 Introduction

1.1 Overview

> Determining the phase equilibria or phase diagram is usually the most important characterization of the macroscopic properties of a colloidal system.[1]
>
> *Evans, Wennerström, 1999*

The properties of a material at specific conditions are given by its phase behavior. Thus the study of the phase behavior is a universal subject for all material scientists. The term "phase" defines a piece of matter of a uniform chemical composition and physical state.[2] Transitions of one phase to another are functions of intensive parameters such as temperature or concentration, that are independent of the system size. They are graphically illustrated in phase diagrams, where phase boundaries mark the thermodynamic equilibrium of two phases. In order to investigate the phase behavior one should determine first the number of components, second the number of phases, and third the nature and composition of each phase over a wide range of intensive parameters.

Poly(2-oxazoline)s are immensely versatile in their chemistry and phase behavior. One repeating unit consists of atoms of the polymer backbone (-(CH_2-CH_2-N)-) and an *N*-acyl substituent. The polymers are obtained from 2-oxazolines through living polymerization. This ensures excellent control over the molecular weight, polydispersity and end groups. The *N*-acyl substituent, the molecular weight, and the nature of the end groups set the phase behavior.

Thermal transitions of poly(2-oxazoline)s have been studied in the bulk, in solutions, and in dispersions. In the bulk, poly(2-oxazoline)s are amorphous or semi-crystalline polymers depending on the *N*-acyl substituent. They may also exhibit sharp thermal transitions in aqueous solutions and crystallize in the heated aqueous medium. Poly(2-oxazoline)s are also used to stabilize multicomponent dispersions with a "smart" response behavior.

Poly(2-oxazoline) are converted from the bulk into solutions or dispersions by the addition low molecular weight and/or polymeric components. In this thesis it will be shown how the properties observed in each of the three states are related to each other. The key questions to be addressed are: Do the components mix and under which conditions? How does the addition of a new component affect the thermal transitions of the poly(2-oxazoline)? Do the same types of transitions take place when a new component is added?

Scheme 1 gives an overview over the thesis contents. The roman numerals at the corners of the triangle refer to three publications devoted respectively to solutions, the bulk state, and dispersions of poly(2-oxazoline)s. Three poly(2-oxazoline)s bearing saturated propyl substituents, namely poly(2-n-propyl-2-oxazoline) (PnPOx), poly(2-isopropyl-2-oxazoline) (PiPOx) and poly(2-cyclopropyl-2-oxazoline) (PcyPOx) were investigated. Publication I focuses on the phase behavior of PnPOx, PiPOx and PcyPOx in water and in water/methanol mixtures of variable composition. All three polymers are soluble in cold water and phase

separate upon heating. In the presence of methanol the phase transition temperature of the mixed solutions varies characteristically for each poly(2-propyl-2-oxazoline) (PPOx).

Publication II describes the bulk properties of PiPOx, block copolymers (BCPs) of PiPOx and poly(lactide) (PiPOx-*b*-PLA), and of blends of PiPOx and PLA. A key finding is that the PiPOx-*b*-PLA BCPs are miscible in the bulk. Particular attention is payed to the influence of miscibility on the crystallization properties of the two polymers and of the BCPs.

Publication III focuses on aqueous dispersion of the block copolymers described in publication II. As PLA is insoluble in water, PiPOx is drawn between two immiscible phases – the dispersed PLA phase and the continuous water phase. The particle morphology and thermal response of PiPOx-*b*-PLA dispersions depends on the molecular weight and the PLA stereochemistry.

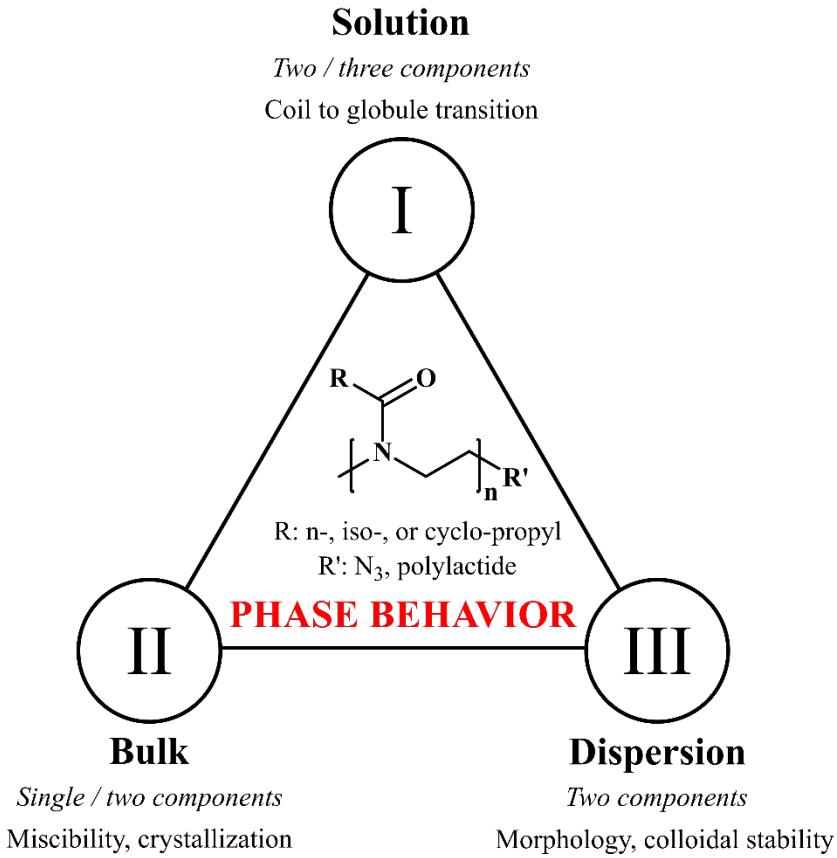

Scheme 1 *Overview of the thesis content organized based on the nature of the poly(2-oxazoline) phases. The original publications are referred to by the roman numerals in the corners of the triangle. The synthesis of the polymers is discussed next.*

1.2 Synthesis of Poly(2-propyl-2-oxazoline)s

> Any growth requires food, and the food for a growing polymer is the monomer.[3]
>
> *Szwarc, 1956*

It took ten years after Swarc coined the term “living polymers”,[3] until four independent research groups reported the living cationic ring-opening polymerization (CROP) of 2-oxazolines.[4–7] The versatility of the emerging poly(2-oxazoline)s chemistry was demonstrated in these early publications in which 23 2-oxazoline monomers were polymerized using various initiators. Also, copolymerization and cross-linking were reported.

Living CROP of 2-oxazolines is a chain-growth polymerization involving initiation and propagation, driven by the isomerization of the cyclic imino ether monomer to a tertiary amide.[8,9] Mechanistically, CROP is initiated by creating an oxazolinium cation and it propagates by the reaction of this cation with the nucleophilic nitrogen atom of another monomer (Scheme 2). The living chain-ends are terminated intentionally by addition of a nucleophile stronger than the monomer. Under appropriate conditions initiation is fast and chain breaking reactions are negligible, leading to first-order kinetics and a linear increase of the degree of polymerization (*DP*) with the monomer conversion. The breadth of polymers obtained is limited by stringent purity requirements of all reactants including monomer, initiator and solvent as well as problems related to unsuitable functional groups that lead to chain transfer, termination or prevent the polymerization entirely.[10] Several reviews are devoted to the polymerization process of 2-oxazolines.[11–13] The following paragraphs give a brief overview.

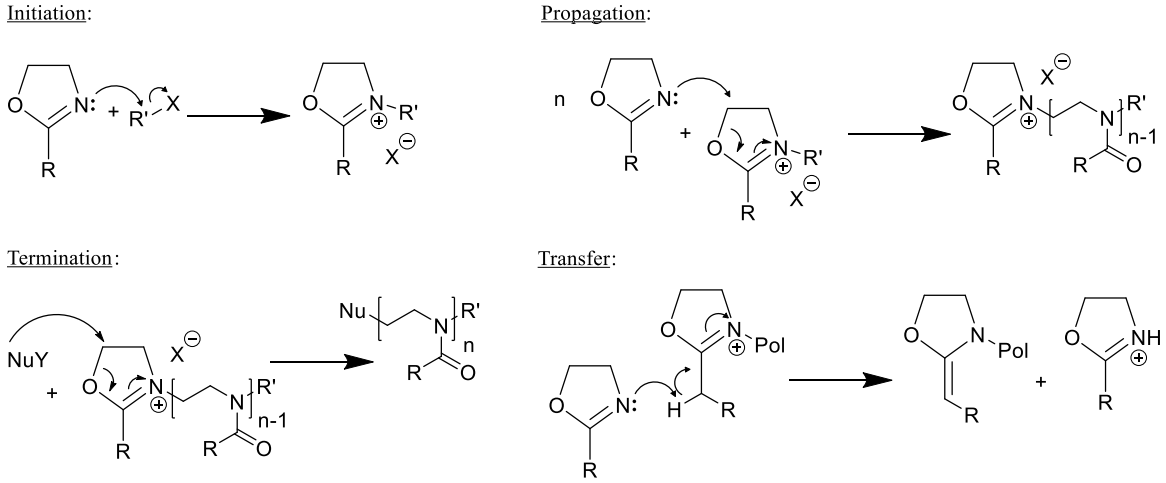

Scheme 2 *Mechanism of the cationic ring opening polymerization (CROP) of 2-oxazolines including initiation, propagation, termination and transfer reactions.*

In the first step of CROP, the nitrogen free-electron pair undergoes a nucleophilic attack with an electrophile to form an oxazolinium cation, the initiating species of CROP. Methyl

p-toluenesulfonate is frequently used as initiator. Also suitable are freshly prepared oxazolinium tosylate salts, which can be isolated and crystallized conveniently.[14] It is possible to introduce functional chain-ends to the polymers during the initiation step by using initiators containing unsaturated hydrocarbons or (protected) heteroatom moieties.[13]

The oxazolinium-cation is attacked at the 5-position by the free electron pair of the nitrogen atom of another monomer to open the ring and propagate the polymerization. The apparent rate of polymerization depends on the monomer, the solvent, and the counter-ion.[11] For the series 2-isopropyl-2-oxazoline (iPOx), 2-n-propyl-2-oxazoline (nPOx), and 2-cyclopropyl-2-oxazoline (cyPOx) polymerized in acetonitrile with methyl *p*-toluenesulfonate as initiator, the polymerization rate is the fastest for the electron withdrawing cyPOx and the slowest for the electron donating iPOx.[15] This is ascribed to the higher nucleophilicity of cyPOx compared to iPOx.[16] The effects of solvent polarity and counter-ion nucleofugality were studied in detail for the polymerization of iPOx.[17] The polymerization rate is generally slower in acetonitrile than in chlorobenzene. In the polar solvent the oxazolinium cation exists as free ion and there are no specific counter-ion effects. In a nonpolar solvent, the oxazolinium- and the counter-ion form an ion-pair and the polymerization rate is sensitive to the nucleofugality of the counter-ion. The fastest propagation rate of iPOx was observed for the system chlorobenzene/ methyl trifluoromethyl sulfonate.

The chain propagation is terminated by addition of a nucleophile, which binds covalently to the oxazolinium cation. The most common quenchers are potassium hydroxide/methanol or potassium hydroxide/water mixtures, which leads to a hydroxyl end-group. The termination step is another handle to introduce functional end-groups. For example addition of sodium azide to living poly(2-oxazoline)s produces polymers with azide end-groups, that can be modified further.

Transfer reactions cannot be excluded entirely. They depend on the solvent, monomer and counter-ion. The most important transfer reaction is ß-elimination of a proton of the 2-substituent leading to the formation of an enamine and a proton-initiated new growing chain. Enamines are weak nucleophiles and can compete with the monomer for chain propagation at high conversions, leading to star-like poly(2-oxazoline)s.

Synthesis of 2-oxazolines:

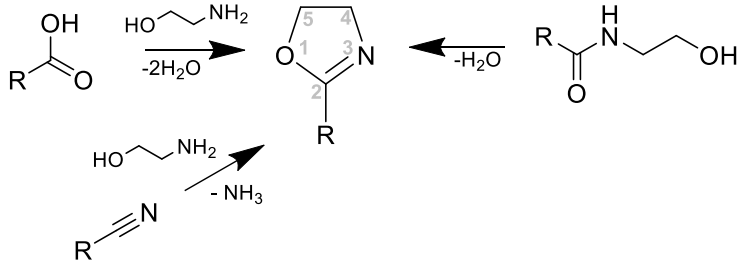

Scheme 3 *Synthetic routes to 2-oxazolines using carboxylic acids, nitriles, or N-acyl-2-aminoethanols as starting materials.*

Cyclic imino ethers, known as 2-oxazolines, are obtained by condensation reactions from compounds such as carboxylic acids, nitriles, or *N*-acyl-2-aminoethanols (Scheme 3).[18] By convention, the numeral 2 marks the position of the double bond in the heteroatom 5-membered ring. The substituent on the 2-position can be a linear, branched, cyclic, (un)saturated, aromatic or fluorinated hydrocarbon.[7] Also 2-oxazolines carrying functional heteroatom substituents can be polymerized but might require suitable protection strategies.[19–21]

1.3 Phase behavior of Poly(2-propyl-2-oxazoline)s

1.3.1 Thermodynamics

1.3.1.1 Flory-Huggins theory of polymer solutions

The theory of polymer solutions was derived independently by Flory (1942)[22] and Huggins (1942).[23–25] It is based on the mean field theory of *ideal* liquid mixtures as described in Raoult's law. In an ideal binary mixture the partial pressure of each component is equal to the product of its mole fraction and the vapor pressure of the pure component. The components do not interact and the enthalpy contribution to the free energy of mixing is zero. *Regular* mixtures of two low molecular weight liquids deviate from Raoult's law due to additional enthalpic effects. Polymer solutions deviate also from Raoult's law but for entropic reasons as will be shown in the following.

Both the Raoult's law and the Flory-Huggins theory deal with binary systems of compounds *A* and *B* consisting of $n_A + n_B = n$ moles. The mole fractions x_A and x_B are given by the equation $x_A + x_B = 1$. The theories can be expanded to ternary systems (two polymers – one solvent, one polymer – two solvents).[26,27] This requires the introduction of additional binary interaction-parameters and the mole fractions are related by $x_A + x_B + x_C = 1$. For the sake of brevity these cases are not discussed here.

Consider first an ideal system of two low molecular weight liquids of identical molecular volume.[28] The heat of mixing $\Delta_M H$ is zero when the nearest neighbor pair interactions w_{AA}, w_{BB}, and w_{AB} cancel each other. Then the free energy of mixing $\Delta_M G = \Delta_M H - T\Delta_M S$ depends only on the entropy, which is given by:

$$\Delta_M S/n = - R\{x_A \ln x_A + x_B \ln x_B\}$$

Eq. (1)

Here, *R* is the universal gas constant. By definition both logarithmic terms are negative and mixing always results in an increase of entropy. In regular solutions the formation of *A*-*B* contacts at the expense of the *A*-*A* and *B*-*B* pairs results in a non-zero heat of mixing:

$$\Delta_M H/n = ßx_A x_B$$

Eq. (2)

ß results from the sum of *A-B*, *A-A*, and *B-B* pair interactions and can be obtained from the energies of vaporization of *A* and *B*, respectively. Combining equations 1 and 2 gives the free energy of mixing, which is graphically illustrated in Figure 1 A:

$$\Delta_M G/n = ßx_A x_B + RT\{x_A \ln x_A + x_B \ln x_B\}$$

Eq. (3)

For a solution of polymer *B* in a solvent *A* the molar volumes of the compounds differ significantly. It is required to use the volume fractions ϕ_A and ϕ_B instead of the mole fractions to calculate the entropy of mixing:

$$\Delta_M S/n = -R\{\phi_A \ln\phi_A + \phi_B/v_B \ln\phi_B\}$$

Eq. (4)

The important difference between equations 4 and 1 is that the pre-factor of the second logarithmic term in equation 4 is divided by the molar volume of the polymer v_B. This is a considerably large number for polymers. The consequence is a comparably small entropy gain for polymer solutions. Equation 4 can be modified to apply also for polymer blends (a binary mixture of two polymers).[29] In this case both logarithmic pre-factors are divided by the molar volume of the respective polymers. This reduces the entropy even more:

$$\Delta_M S/n = -R\{\phi_A/v_A \ln\phi_A + \phi_B/v_B \ln\phi_B\}$$

Eq. (5)

The heat of mixing of polymer solutions is given by:

$$\Delta_M H/n = -RT\chi_{AB}\phi_A\phi_B$$

Eq. (6)

with the interaction parameter χ_{AB}:

$$\chi_{AB} = z\Delta w_{AB}/RT$$

Eq. (7)

Here z is the coordination number and the balance of pair interactions is:

$$\Delta w_{AB} = w_{AB} - 1/2\ (w_{AA} + w_{BB})$$

Eq. (8)

Finally, the free energy of mixing for polymer solutions and polymer blends results from combining equations 4 and 6, or respectively 5 and 6:

$$\Delta_M G/n = RT\{\phi_A \ln\phi_A + \phi_B/v_B \ln\phi_B + \chi_{AB}\phi_A\phi_B\}$$

Eq. (9)

$$\Delta_M G/n = RT\{\phi_A/v_A \ln\phi_A + \phi_B/v_B \ln\phi_B + \chi_{AB}\phi_A\phi_B\}$$

The consequence of the low entropy of mixing for polymer solutions and even more for polymer blends is that the heat of mixing becomes the decisive factor for miscibility (see next section). One shortcoming of the original Flory-Huggins theory is the assumption that the nearest neighbor interactions are isotropic and have only an enthalpic contribution. However, the pair interactions reduce the translational freedom of the partners and affect the entropy of the system. Thus, the χ-parameter is the sum of enthalpic and entropic contributions and is temperature dependent.[29] In reality $\Delta_M H$ and $\Delta_M S$ can be both positive and negative quantities. What results is a delicate temperature-dependent balance of the entropic and enthalpic contributions.

1.3.1.2 Phase transitions

The general conditions for miscibility are (I) a negative free energy of mixing $\Delta_M G$ and (II) a positive curvature of $\Delta_M G$ as function of the composition x_A ($\partial^2 \Delta_M G / \partial x_A^2 > 0$). The second condition is important when the heat of mixing exceeds a critical positive value ($ß > ß_c$, or $\chi > \chi_c$). Consider first the case of an ideal mixture of two low molecular weight liquids (Figure 1 A, equation 3, with $ß = 0$). A plot of $\Delta_M G$ vs x_A is parabolic and goes through a minimum at $x_A = 0.5$. Mixing occurs at all compositions. For $ß > ß_c$ the curve exhibits two minima and a central maximum at $x_A = 0.5$. The minima are known as the binodal points ($\partial \Delta_M G / \partial x_A = 0$). The inflection points are the spinodal points ($\partial^2 \Delta_M G / \partial x_A^2 = 0$). All systems with compositions between the two spinodal points ($\partial^2 \Delta_M G / \partial x_A^2 < 0$) are unstable and phase separate by coarsening of a bicontinuous phase (spinodal decomposition). Systems with compositions between the spinodal and binodal points are meta-stable towards concentration fluctuations and phase separate via a nucleation and growth mechanism. For blends of two polymers with the same molar volume ($v = v_A + v_B$) the value of χ_c is inversely proportional to v. It follows that for such systems phase separation is the standard case and miscibility is a rare exception. The latter takes place when the heat of mixing is negative, in particular when attractive electrostatic interactions, hydrogen bonding or dipole-dipole interactions exist. It should be noted that for polymer solutions the molar volumes of solute and solvent are drastically different. Thus the free energy function becomes asymmetric and the maximum shifts to a solvent rich composition.

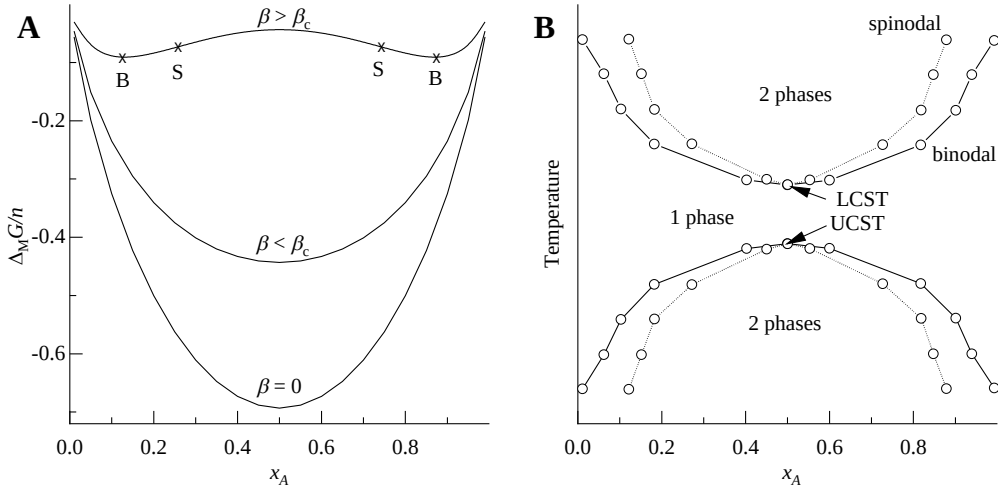

Figure 1 *(A) Free energy of mixing of two low molecular weight liquids as function of the mole fraction x_A for different values of ß. (B) Temperature – composition diagram showing the dependence of the binodal (—) and spinodal (···) points. UCST and LCST are indicated with arrows.*

Spinodal and binodal points can be plotted in a temperature – composition phase diagram (Figure 1 B). Depending on the balance of thermodynamic contributions a homogeneous solution can demix either upon cooling or heating. The shared point of the binodal and spinodal curves denotes in the former case the upper critical solution

temperature (UCST) and in the latter case the lower critical solution temperature (LCST). Above the UCST or below the LCST the components mix at all compositions.

1.3.1.3 Polymer crystallization

Polymers with a suitable chemical structure can undergo a phase transition from an unordered to a semi-crystalline state. The term semi-crystalline accounts for the fact that a polymer is never 100 % crystalline. Rather, it is a semi-crystalline material consisting of amorphous and crystalline phases. Crystallization involves a conformational transition of the polymer chains. In the molten state the chains adopt a random coil conformation. Cooling below this temperature leads to the formation of extended segments with increased order. These segments are interrupted by regions of low order. The extended segments align in parallel, held together by non-covalent forces and grow in lateral dimensions. Several of such crystalline sheets stack and are separated by the amorphous regions. It is possible that these stacks form superstructures, which can be observed under the optical microscope.

Polymer crystallization is kinetically controlled due to the slow diffusion of the high molecular weight compounds.[30–32] It is limited to the temperature range between the glass transition temperature, T_g, and the equilibrium melting temperature $T_m°$. The melting temperature T_m increases with the thickness of the crystalline sheets and would reach $T_m°$ for infinitely thick crystallites. The finite thickness of the crystalline sheets increases with the crystallization temperature T_c. Thus, $T_m°$ of a given polymer can be obtained by plotting T_m as a function of T_c by extrapolation to the line $T_c = T_m$. At $T_m°$ the rate of melting equals the rate of crystallization. At a temperature slightly below $T_m°$ the degree of undercooling ($\Delta T = T_m° - T_c$) is low. It follows that the nucleation rate is slow and crystallization is hardly observed. At temperatures slightly above T_g, the observed crystallization rate is low due to the slow diffusion of the polymer chains. The crystallization rate is the highest in the intermediate temperature range between T_g and $T_m°$. The crystallization rates can be increased by adding nucleating agents or plasticizers. The first type of additives aim to enhance the melt with heterogeneous surfaces as nucleation sites. Plasticizers increase the chain mobility and the T_g shifts to lower temperatures. The presence of plasticizers can affect $T_m°$ and therefore the nucleation process.[33]

1.3.2 Phase behavior of Poly(2-oxazoline)s in solution

The solubility of poly(2-oxazoline)s in water and organic solvents depends on the *N*-acyl substituent. A good overview of the poly(2-oxazoline) solution properties is given in several review articles.[12,34,35] The most attention is devoted to aqueous poly(2-oxazoline)s solutions. Poly(2-methyl-2-oxazoline) (PMeOx) is soluble in water at all temperatures, while poly(2-ethyl-2-oxazoline) (PEtOx),[36] PiPOx,[37] PcyPOx[15] and PnPOx[38] dissolve in cold water. Their solutions phase separate upon heating at a characteristic temperature (T_{trans}). Poly(2-butyl-2-oxazoline) and higher homologues are not soluble in water.

The transition from a homogeneous to a heterogeneous system upon heating aqueous solutions of some poly(2-oxazoline)s is driven by thermodynamics. Attractive polymer-water interactions contribute with a negative sign to the Gibbs free energy ($\Delta_M H < 0$). These attractive interactions are counterbalanced by a decrease of translational entropy ($\Delta_M S < 0$) of the bound solvent molecules. With increasing temperature the $-T\Delta_M S$ term becomes dominant and the Gibbs free energy turns positive, which causes the release of the bound water and the coil-to-globule transition. The globules form a polymer-rich dispersed phase with a different refractive index than the bulk water and the sample turns turbid. Experimentally, the most common techniques to detect the phase transition are transmittance measurements and high sensitivity differential scanning calorimetry (µDSC). The first technique gives the cloud point temperature (T_{CP}) of the solution. The second technique measures the heat transfer during heating which passes through a maximum at T_{max}. T_{CP} and T_{max} are not identical for a given solution as different physical properties are probed in the two measurements. For some polymers the change of transmittance and the endotherm take place in a narrow temperature range. In this case the transition is an all-or-none process. The theoretical model for this behavior was derived by Tanaka, F.[39,40] According to this model the hydration of one repeating unit by a molecule of water causes the reorientation at the neighboring repeat unit, and facilitates the formation of long sequences of bound water molecules along the polymer chain. The transition broadens when the hydration cooperativity is disturbed.

The transition temperature of thermo-responsive poly(2-oxazoline) solutions depends on the polymer concentration. The minimum of the demixing curve in a temperature vs. concentration phase diagram defines the lower critical solution temperature (LCST). At constant polymer concentration, T_{trans} decreases with increasing molecular weight (PEtOx,[36,41,42] PnPOx[41] and PiPOx[43]). PEtOx[41] (*DP* 100) and PiPOx[44] (*DP* 17) exhibit a T_{trans} of above 100 °C and 73 °C (1 g/L), respectively. T_{trans} can be adjusted between 20 and 80 °C by copolymerization of different 2-oxazolines.[38,41,45,46] Also the chain architecture has an influence on T_{trans} as shown for star-like,[47] comp-like,[44] and cyclic[48] poly(2-oxazoline)s in comparison to linear ones.

The solution behavior is affected by addition of salts[36,49] and cosolvents.[50] The latter case is of particular interest. Different thermo-responsive polymers exhibit contrasting trends of T_{trans} when a second good solvent, such as methanol, is added to the aqueous solution. T_{trans} of poly(vinyl methylether) in water increases continuously with increasing methanol content.[51] Solutions of poly(*N*-isopropyl acrylamide) (PNIPAM) in water/methanol mixtures of 5 - 35 mol% methanol exhibit the opposite trend, T_{trans} decreases.[51,52] This behavior was termed cononsolvency and several theories have been proposed to explain the phenomenon. The central arguments in the ongoing debate are: competitive H-bonding of water and methanol molecules, which leads to a loss of the hydration cooperativity and the formation of unsolvated sequences along the polymer chain,[53,54] geometric frustration,[55] changes of the chain conformation in the coil and the globular state in the presence of methanol,[56,57] bridging interactions of preferential bound methanol molecules,[58,59] or the energetic states of free and bound water.[60,61] Some authors see an important role in the H-bond donor ability of PNIPAM. They compare the phase

behavior of PNIPAM in water/methanol mixtures to the behavior of thermo-responsive polymers which lack the ability to act as a H-bond donor.[62]

The balance of polymer-polymer and polymer-solvent interactions is important for the discussion of PiPOx-*b*-PLA BCP dispersions. In this respect it is interesting to note the solution behavior of PEtOx and poly(acrylic acid) (PAA) in water and organic solvents.[36] When these two polymers are dissolved separately in water and the two solutions are mixed, strong H-bonding interactions cause precipitation of a complex. The same is observed for solutions in methanol and dioxane, but not when dimethyl sulfoxide is used as solvent. The yield of precipitated polymer depends on the ratio of PEtOx and PAA and is nearly 100% at 42 mol% PEtOx. The stoichiometry in the complex varies with the composition of the mixed solutions. The T_g of the complex after drying is a measure of the amount of H-bonds formed. It depends on the PEtOx/PAA ratio and is higher than the T_gs of the pure components, when the complex is formed in water or methanol. The T_g is lower when the complex is prepared from dioxane solutions and is constant irrespective the PEtOx/PAA ratio. The peculiar solvent effect is explained by the different pair interactions in the tertiary mixtures.[36]

Aqueous solutions of PiPOx crystallize when the sample is kept above T_{trans} for prolonged times. The crystal structure observed by wide angle x-ray scattering (WAXS) is identical to that obtained after crystallization in the bulk (see section 1.3.3.2).[63] The crystalline phase consists of nano-fibers, which assemble in spherical micron-sized objects.[64] The morphology depends on the temperature and can be modified by addition of cosolvents and surfactants. The mechanism of crystallization involves first the coil-to-globule transition, which is followed by liquid-liquid phase separation. The formation of a bicontinuous phase of a vitrified sample at $T > T_{trans}$ was observed by cryogenic scanning electron microscopy.[64] Observations by optical microscopy revealed that the crystallization takes place in the polymer rich liquid phase.[65] On the molecular level IR-spectroscopy and molecular modeling indicated that the PiPOx main-chain transforms into an all-trans conformation at $T > T_{trans}$ prior to the crystallization.[65] The oriented dipoles guide the growth of the crystal.[63,66,67]

1.3.3 Phase behavior of Poly(2-oxazoline)s in the bulk

1.3.3.1 Miscible Poly(2-oxazoline) blends

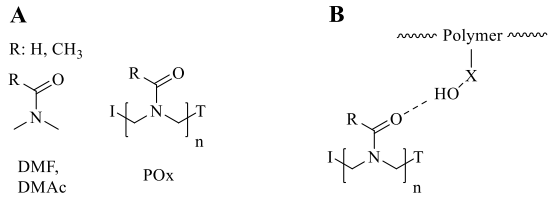

Scheme 4 *(A) Chemical similarity between the solvents DMF and DMAc and poly(2-oxazoline)s. (B) H-bonding interaction between a poly(2-oxazoline) and a polymer listed in Table 1.*

Material properties can be tuned by blending different polymers. For this purpose the phase behavior of the two- or multicomponent systems needs to be understood, in particular the nature of interactions between the components. Poly(2-oxazoline)s display structural analogies to *N*,*N*-dimethylformamide (DMF) and *N*,*N*-dimethylacetamide (DMAc) (Scheme 4 A). Both the polymer and the low molecular weight compounds contain a dipolar tertiary amide bond and interact similarly with other components. DMF and DMAc are good solvents for many polymers. Also poly(2-oxazoline)s are compatible with a number of polymers and form miscible blends over a limited or the entire composition range. Table 1 lists polymers miscible with PMeOx and PEtOx. The listed polymers have in common the ability to act as H-bond donor. They form H-bonds with the carbonyl-oxygen of the poly(2-oxazoline)s (Scheme 4 B).[36] The interactions of the H-bond donor polymers with PMeOx are stronger than with PEtOx, as inferred from the shifts of the C=O stretching vibration observed by FT-IR spectroscopy.[68] The H-bonds act as physical cross-links between the interacting polymer chains. The T_g of the blend may be higher than that of the pure components.[36] PMeOx is also miscible with poly(vinyl chloride) (PVC) and poly(vinylidene fluoride) in blends of less than 50 wt% poly(oxazoline) content.[69] Random copolymers exhibit an interaction parameter different from that of a blend of the respective homopolymers.[70] Random copolymers of styrene and acrylonitrile with an acrylonitrile content of 20-40 wt% are miscible with PEtOx over the entire blend composition range, while poly(styrene) and poly(acrylonitrile) are immiscible with PEtOx.[71]

Table 1 *Investigated H-bond donor polymers forming miscible blends with poly(2-methyl-2-oxazoline) and poly(2-ethyl-2-oxazoline)*

Polymer	*Reference*
Poly(acrylic acid) (PAA)	36
Poly(vinyl alcohol) (PVA)	72,73
Poly(vinyl phenol) (PVPh)	36,68,74
Poly(hydroxyethyl methacrylate)	75
Poly(hydroxypropyl methacrylate)	68,75
Poly(hydroxyether) of bisphenol A	68,71
Poly(ethylene-co-methacrylic acid)	76

Poly(2-oxazoline)s were used to combine biopolymers with incompatible synthetic polymers. Chitin is an abundant biopolymer with potential for medical applications but suffers from poor solubility and processability. Chitin grafted with PMeOx and PEtOx exhibits enhanced solubility. Solution cast films prepared of the graft copolymers mixed with either PVA or PVC exhibit a single T_g and are miscible.[72,73,77] In the same manor cellulose grafted with PMeOx[78] and lignin grafted with PEtOx[79] form homogeneous films with PVC. Block copolymers consisting of a PMeOx or PEtOx block and a poly(ethylene glycol) or poly(dimethyl silane) block were used to modify the electrostatic properties of Nylon6[80,81] and poly (vinyl chloride)[82] fibers. The poly(2-oxazoline) block acted as compatibilizer.

1.3.3.2 Crystallization of Poly(2-oxazoline)s

The T_g of poly(2-alkyl-2-oxazoline)s depends on the alkyl-chain length. In the series of linear saturated alkyl-chains it decreases linearly from ~80 °C (2-methyl) to ~ -10 °C (2-hexyl), due to the increasing segment flexibility.[66] The T_gs of PPOxs follow the order PcyPOx > PiPOx >> PnPOx, reflecting the rigidity of the propyl-group.[15]

Litt reported in 1969 a detailed x-ray study of crystalline poly(2-alkyl-2-oxazoline) fibers.[83] Poly(2-alkyl-2-oxazoline)s containing an isopropyl- or alkyl-substituents with four or more carbon atoms are semi-crystalline. There exist conflicting reports, whether PMeOx and PnPOx are semi-crystalline or not.[7,66]

Generally, semi-crystalline poly(2-alkyl-2-oxazoline)s crystallize in a triclinic unit cell containing two repeating units. The -CH_2-CH_2-N-CH_2-CH_2-N- main chain is twisted and runs along the c-axis with a periodicity of 6.4 Å. The side-chains are tilted by 54 ° from the c-axis and the periodicity along the b-axis increases by 2 Å per CH_2 group of the 2-alkyl substituent. Over the years the interpretation of x-ray diffraction data has changed concerning the precise crystal structure of PiPOx. Originally, Litt assumed a planar orientation of all side-chains, which alternate to either side of the main chain. Recently, Demirel proposed a helical orientation of the side-chains with a pitch length of 15 repeating units.[67]

The T_m and crystallization kinetics depend strongly on the alkyl-substituent. Slow crystallization is observed for PiPOx, while poly(2-hexyl-2-oxazoline) and higher homologs crystallize more rapidly. This is attributed to the increasing distance between neighboring chains and the decreasing dipolar interactions between the amide groups as the side-chain length increases.[66] These interactions are viewed as physical cross-links between chains, which limit the chain flexibility and therefore restrict the transformation to the highly ordered semi-crystalline phase. Poly(2-oxazoline)s with 2-hexyl and longer side-chains have a T_m around 150 °C, that decreases with increasing side-chain length. PiPOx has an exceptionally high melting temperature of around 200 °C ascribed to the denser packing and stronger dipole interactions.

1.3.4 Phase behavior of Poly(2-oxazoline) dispersions

Amphiphilic polymers form colloidal dispersions in water.[84] According to Hadjichristidis a fundamental study of the micelle formation should address “the structure of an isolated micelle and […] the configuration of a (individual) block copolymer chain incorporated in a micelle.”[85] Spherical, cylindrical and vesicular particle morphologies have been observed, depending on the molecular properties of the BCP and the solvent selectivity.[86] The particle preparation process has an important effect on its morphology.[87,88] Dispersions are stabilized by a delicate balance of interactions. Solvophobic polymer segments associate in the core of the particles to avoid unfavorable contact with the continuous phase. Macroscopic phase separation of the insoluble material is prevented by the soluble polymer segments that remain on the particle shell. In this micellization scheme the solvophilic and

solvophobic polymer blocks segregate in the core and the shell of the micelle. The particle structure is given by the volume fractions of the blocks. The situation is modified when the segregating forces are opposed by attractive interactions between the two blocks.[89] For example oppositely charged polyelectrolytes undergo interpolyelectrolyte complexation and form multicompartment micelles.[90–92]

Poly(2-oxazoline) stabilized dispersions in water have created a flow of publications in the recent years.[93,94] The heterogeneous dispersions can stabilize active ingredients that are insoluble in the continuous phase. This is of particular interest for nanomedical applications in which altered pharmacokinetics and tissue specific targeting are desirable. The properties of poly(2-oxazoline)s in biological environments are often compared to those of poly(ethylene glycol) (PEG), the gold standard polymer for biomedical applications.[95–99] Undesired side-effects of PEG were observed in some patients recently, urging the search for alternative polymers.[97,98] A clinical trial of a PEtOx-protein conjugate for the treatment of Parkinson's disease was started in 2015.[100–102] Poly(2-oxazoline)s fulfilling the molecular requirements to self-assemble in water are easily obtained. BCPs exclusively build from 2-oxazoline monomers can be produced by sequential monomer addition. Chain extension with other types of monomers or polymer-polymer coupling reactions are feasible by the choice of initiator and terminating agent.[13] Driven by the versatility of the poly(2-oxazoline) chemistry, numerous examples of particle dispersions have been studied on the fundamental and applied level.

One challenge for nanomedical applications concerns the degradability of the polymeric materials under physiological conditions. Poly(lactide) (PLA) is a biodegradable aliphatic polyester used as biomaterial in various applications.[103,104] Lactide, the cyclic diester of lactic acid, exhibits two stereo-centers and therefore exists in the form of three isomers: (*S,S*)-lactide (*L*-lactide), (*R,R*)-lactide (*D*-lactide), and (*R,S*)-lactice (*meso*-lactide). Polymerization of L-lactide or D-lactide produces a stereo-regular semi-crystalline polymer: PLLA and PDLA. The stereo-irregular, amorphous polymer PDLLA is obtained by polymerization of *meso*-lactide or a racemic mixture of *L*- and *D*-lactide.

Several reports discuss fundamental and applied questions related to dispersions of BCPs consisting of a PMeOx or PEtOx block and a PLA block.[105–112] Some authors characterized the micelles of PEtOx-*b*-PLLA by fluorescence techniques[105] and NMR spectroscopy,[107] based on the assumption that PEtOx and PLLA phase separate strictly. Addition of PAA to the PEtOx-*b*-PLLA micelles at pH < 3.5 leads to complexation between PAA and PEtOx and causes precipitation.[105] The PAA – PEtOx attraction ceases when the pH exceeds 3.8 and the micelles redisperse. Micelles of PEtOx-*b*-PLA were loaded with doxorubicin,[107] paclitaxel,[109] a vitamine E derivative,[110] and agents for photodynamic therapy[112] to demonstrate the potential of these BCP micelles for drug delivery applications. Le Fer et al investigated PMeOx-*b*-PDLLA particles prepared by the rapid solvent exchange method.[111] The particles were analyzed by dynamic light scattering, cryogenic transmission electron microscopy (cryoTEM) and small angle neutron scattering (SANS). The hydrophilic weight fraction of the BCPs ranged from 30 to 66 %. Surprisingly for such a wide range of compositions the BCPs assembled into spherical particles irrespective of the hydrophilic weight fraction. The authors conclude that the particle morphology is controlled

by the kinetics of the self-assembly process. The particles consisted of a dense PDLLA-core and a shell of not fully extended PMeOx-chains.

The phase behaviors of a given poly(2-oxazoline) in solution, the bulk state and dispersion – set by the chemistry of the polymer chain – are closely related. Valuable conclusions can be drawn by comparing the phase behaviors in the different states. The miscibility of two polymers is straightforwardly established in the bulk by assessing the T_g-region of the mixture. The cooperativity of the coil-to-globule transition observed in solutions and dispersions of polymers by turbidity and calorimetric measurements is diagnostic of the polymer conformation and the local environment around the chains. The combination of appropriate analysis methods applied to polymers in the different states allows to draw a comprehensive picture of their phase behaviors.

2 Objectives

Poly(2-propyl-2-oxazoline)s exhibit unusual phase behaviors in solution, the bulk and in dispersions. Each of these phases are potential fields of applications of poly(2-propyl-2-oxazoline)s. The objective of this thesis is to bring together fundamental observations made in the different states of matter.

The results are organized in the following chapters:

1. *Synthesis* and molecular characterization of poly(2-propyl-2-oxazoline)s and PiPOx-*b*-PLA with controlled molecular weights and end-groups. [I, II]

2. *Solutions* of poly(2-propyl-2-oxazoline)s in water, in methanol and in water/methanol mixtures; concentrating on the coil-to-globule transition. [I]

3. *Bulk* phase behavior of PiPOx, PLA and PiPOx-*b*-PLA; focus on the miscibility of PiPOx and PLA and the crystallization behavior. [II]

4. *Dispersions* of PiPOx-*b*-PLA in water; aiming to uncover the particle morphology and thermo-responsive behavior. [III]

3 Experimental part

In this section the most important experimental procedures and characterization methods are briefly summarized. Detailed descriptions are available in the respective publications and their supporting information documents.

3.1 Syntheses and molecular characterization

3.1.1 Molecular characterization

The compounds synthesized were characterized by Fourier transform infrared (FT-IR) and nuclear magnetic resonance (NMR) spectroscopy. FT-IR spectra were obtained with a PerkinElmer One FT-IR-spectrometer (1 cm^{-1} resolution) or a Bruker ALPHA P (2 cm^{-1} resolution). Both spectrometers were equipped with an attenuated total reflection (ATR) probe. NMR spectra (^{1}H: 500.13 MHz, ^{13}C: 125.77 MHz) were measured with a Bruker Avance III 500 spectrometer. All spectra were calibrated against the solvent residual proton signal (chloroform-d: 7.26 ppm, deuterium oxide: 4.79 ppm, methanol-d4: 3.31 ppm). The probe temperature was 25 °C unless otherwise noted and controlled with a BCU-05 variable temperature unit. Pulse sequences were used as published in the Bruker pulse program catalog (zg30, zgpg30, ledbpgp2s, noesyphsw). Two-dimensional nuclear Overhauser effect spectra (NOESY) were recorded with the mixing time set to 600 ms. Diffusion ordered spectra (DOSY) were recorded at 10 °C with 32 steps of increasing the linear gradient strength and a diffusion delay of 100 ms. The exponential decays of signal intensities with increasing gradient strength were fitted according to standard equations to obtain the diffusion constants.

The molecular weight distributions of the polymers were obtained by size exclusion chromatography (SEC) or in some cases by time of flight mass spectrometry using the matrix assisted laser desorption/ionization technique (MALDI ToF). SEC elugrams of the polymers eluted with tetrahydrofuran (THF) + 1 % toluene or with *N*,*N*-dimethyl formamide (DMF) + LiBr were acquired using a Waters 515 HPLC-pump (flow rate: 0.8 mL/min) and a Waters 2410 refractive index detector. The polymer samples were fractionated with a set of Waters Styragel HR 2, 4, 6, 7 and 8 columns (300 mm). Their relative molecular weights were calibrated against polymethyl methacrylate or polystyrene standards. MALDI ToF spectra were measured with a Bruker Microflex instrument in reflection mode. The samples containing *trans*-3-indoleacrylic acid, sodium trifluoroacetate and polymer dissolved in THF were prepared by air drying a drop of the mixture on a steel plate.

3.1.2 Syntheses of 2-propyl-2-oxazoline monomers

The monomers 2-n-propyl-2-oxazoline (nPOx), 2-isopropyl-2-oxazoline (iPOx), and 2-cyclopropyl-2-oxazoline (cyPOx) were synthesized according to the method of Witte and Seelinger[114] using different carbonitriles as source of the propyl-substituent. The carbonitrile was reacted at 130 °C with a 1.1 molar excess of ethanol amine in the presence of catalytic amounts of zinc acetate. Ammonia is released. The monomers were isolated by distillation under reduced pressure.

3.1.3 Cationic ring opening polymerization of 2-propyl-2-oxazolines

The monomers were dried over calcium hydride and distilled immediately prior to the polymerization. A mixture of monomer, acetonitrile and methyl trifluoromethanesulfonate was brought to 70 °C under inert atmosphere. The monomer conversion was monitored by ^{1}H NMR spectroscopy of aliquots withdrawn from the reaction flask. When the monomer conversion reached approximately 70-90 %, the living chain ends were terminated by reaction with sodium azide. The PPOxs were isolated by dialysis against water and freeze-drying.

3.1.4 Ring opening polymerization of lactide

L-lactide and DL-lactide were polymerized in the bulk at 110 °C and 130 °C, respectively, in the presence of propargyl alcohol and stannous octoate until complete monomer conversion. The PLAs were purified by precipitation of concentrated solutions in dichloromethane into ice-cold methanol, dissolved in 1,4-dioxane, and isolated by freeze-drying.

3.1.5 Copper catalyzed cycloaddition of PiPOx-azide and PLA-alkyne

PiPOx-*b*-PLA block copolymers (BCPs) were obtained by reacting PLA, a 1.2 molar excess of PiPOx and copper(I)/ N,N,N',N'',N''-pentamethyldiethylenetriamine complex in DMF under inert atmosphere at 50 °C. The catalyst complex was removed by passing the reaction mixture through an aluminum oxide column. The eluted solution contained the BCP and unreacted PiPOx. The solution was dialyzed against pure water and freeze dried. The solids were re-dispersed in water at high concentration. Centrifugation at 14680 rpm (30 min) led to the formation of a BCP pellet. The supernatant containing unreacted PiPOx was discarded.

3.2 Characterization of polymer solutions

3.2.1 Poly(2-propyl-2-oxazoline)s in water and in methanol

Solutions of poly(2-propyl-2-oxazoline)s in water and in methanol were prepared by weighing dry polymer powders and solvent on the balance. The samples were kept at 5 °C over night before any measurement. The solution properties were analyzed by NMR spectroscopy as described in section 3.1.1.

The sample transmittance as a function of the temperature of aqueous solutions was detected by turbidimetry at a wavelength of 400 nm and a path length of 1 cm. Transmittance versus temperature curves were obtained with a CD spectrometer J-815 (Jasco) equipped with a PTC-423S/15 Peltier temperature control system or a UV/vis spectrometer V-750 (Jasco) equipped with a ETCR-762 Peltier cell holder and a CTU-100 circulation thermostat unit. Both instruments detect the temperature (+/- 0.1 °C) with a thermocouple placed inside the solution. The samples were equilibrated at low temperature, typically 10 °C or 20 °C for 10 min and heated to 80 °C with a heating rate of 1 °C/min. In publication I the cloud point temperature (T_{CP}) was defined as the inflection point of the transmittance curve. In publication III T_{CP} was defined as the onset of turbidity determined by the intersection of a tangent at the inflection point and a tangent at maximum transmittance.

Thermograms of the aqueous polymer solutions were obtained with a Malvern Microcal PEAQ-DSC (publication I) or a Microcal VP-DSC (publication III). In both cases the heating rate was 1 °C/min and the instrument operated without active cell-cell compensation. A solvent baseline was subtracted from the sample data and the area under the transition peak was integrated to give the calorimetric enthalpy.

3.2.2 Poly(2-propyl-2-oxazoline)s in water/methanol mixtures

Aqueous and methanolic stock solutions were prepared as described in section 3.3.1 and mixed in appropriate portions as determined by weight. Turbidimetry and µDSC measurements were conducted as described in section 3.3.1.

3.3 Characterization of the bulk properties

3.3.1 Miscibility of PiPOx and PLA

Solubility parameters δ of PiPOx (δ_{PiPOx}: 24.0 $J^{0.5}cm^{-1.5}$) and PLA (δ_{PLA}: 22.7 $J^{0.5}cm^{-1.5}$) were calculated according to the method of Fedors.[115] Differential scanning calorimetry (DSC) experiments were conducted with a TA DSC Q 2000 using the refrigerated cooling system RCS 90. Two mg of freeze dried homopolymer or BCP were loaded into a Tzero aluminum

pan and sealed. The sample pan and an empty reference pan were placed into the calorimetric cell, which was purged with a nitrogen flow (50 mL/min) during the entire operation. The cell was equilibrated at 0 °C for 5 min and a heating/cooling/heating experiment was performed. The glass transition region was examined during the second heating (upper temperature: 215 °C, heating/cooling rate: 10 °C/min). Blends of PiPOx and PLA were analyzed following the same protocol after drop casting a ternary PiPOx/PLA/chloroform solution onto a glass slide and vacuum drying.
Miscibility of the molten BCP samples (215 °C) was investigated by small-angle x-ray scattering (SAXS). The instrument consisted of a Bruker Microstar microfocus x-ray source (CuKα, 1.541 Å), a Montel multilayer focusing monochromator, four collimating slits and a Hi-Star 2D area detector. The sample-detector path of 1.59 m was kept under vacuum to prevent scattering from air. The instrument was calibrated with silver behenate. Intensity versus scattering vector plots were obtained by azimuthal averaging the 2D scattering profile.

3.3.2 Crystallization behavior

Polarized optical microscopy (POM) images were obtained using a JENAPOL polarizing microscope using a Planchromat Pol 10x/0.20 ∞/0 objective and a Canon PC1146 digital camera. The FP82 heating stage was operated with a FP80 central processor. The samples were prepared by drop casting polymer/chloroform solutions onto glass slides. The vacuum dried films were sandwiched between the glass slide and a cover slip, placed into the heating stage and focused between the polarizers of the microscope. The samples were melted at 215 °C for 2 min and the polarizers aligned to minimize the transmitted light. For isothermal crystallization, the temperature was set to 130 °C (cooling rate: 20 °C/min) and held constant until completion of crystallization.

The POM observations were complemented by monitoring the isothermal crystallization calorimetrically. The same equipment and sample preparation as described in section 3.2.1 were used. The samples were kept at 215 °C for 3 min and cooled to the isothermal crystallization temperature (T_c, 80 °C/min). After 2 hours, the samples were heated to 225 °C. Isothermal crystallization of BCPs was investigated only at a T_c of 130 °C. For the PiPOx and PLLA homopolymers, changes of the melting temperature (T_m) as function of T_c were monitored by changing the sample for each T_c.

The crystal structure was analyzed by wide-angle x-ray scattering (WAXS). After isothermal crystallization the brittle polymer films were detached from their substrate and placed as powders between two Mylar^{TM} foils. Each sample was measured for 45 min. The instrument consisted of an x-ray tube (PANalytical), a generator (Seifert), a Montel multilayer monochromator to select the wavelength of CuKα irradiation and a 2D Mar345 detector.

3.4 Preparation and Characterization of dispersions

Aqueous dispersions of PiPOx-*b*-PLA were prepared by dissolving a BCP in tetrahydrofuran (THF) (10 g/L, 0.5 mL), a common solvent for PiPOx and PLA. This solution was added dropwise to de-ionized water (2.5 mL), which was stirred moderately. THF was allowed to evaporate at room atmosphere. Subsequently traces of THF were removed by dialysis. The recovered aqueous BCP dispersion was diluted by addition of water to reach a BCP concentration of 0.5 g/L, unless otherwise noted. The dispersion was filtered 11 times each through track-etched membranes with pore sizes of 400 nm, 200 nm, and 100 nm using an Avanti Polar Lipids miniextruder.

Concentrated dispersions (25 g/L) of BCPs in D_2O were analyzed by ^1H NMR spectroscopy as outlined in section 3.1.1. The response to temperature changes of the dispersions were investigated by turbidimetry and µDSC as described in section 3.3.1.

The particle size and morphology were analyzed by combined dynamic and static light scattering using an instrument consisting of a Coherent Sapphire 488-100 CDRH laser, a Brookhaven Instruments goniometer BIC-200SM, a BIC-CrossCorr detector and a BIC-TurboCorr digital auto/cross-correlator.

Dispersions of BCPs in D_2O (10 g/L) were characterized by small-angle neutron scattering performed on the JEEP II reactor at IFE, Kjeller, Norway.

BCP dispersions were vitrified for cryo-TEM analysis with a Leica EMGP vitrification device and observed with a FEI Talos Arctica microscope (200 kV) equipped with a Falcon 3 camera at a magnification of 57000.

4 Results and Discussion

4.1 Polymer synthesis

The poly(2-oxazoline)s were synthesized by CROP of iPOx, nPOx, or cyPOx using methyl trifluoromethanesulfonate as initiator. The absence of chain cleavage reactions was confirmed in the case of PiPOx1-3 by the linear dependence of -ln(1-X_p) as function of the polymerization time (Figure 2 A) and M_n as function of the monomer conversion (X_p, Figure 2 B). The polydispersity (M_w/M_n) of the growing chains was constant with values between 1.1 and 1.3 (Figure 2 C). When X_p reached 70-90 % the living chain ends were terminated by addition of sodium azide.

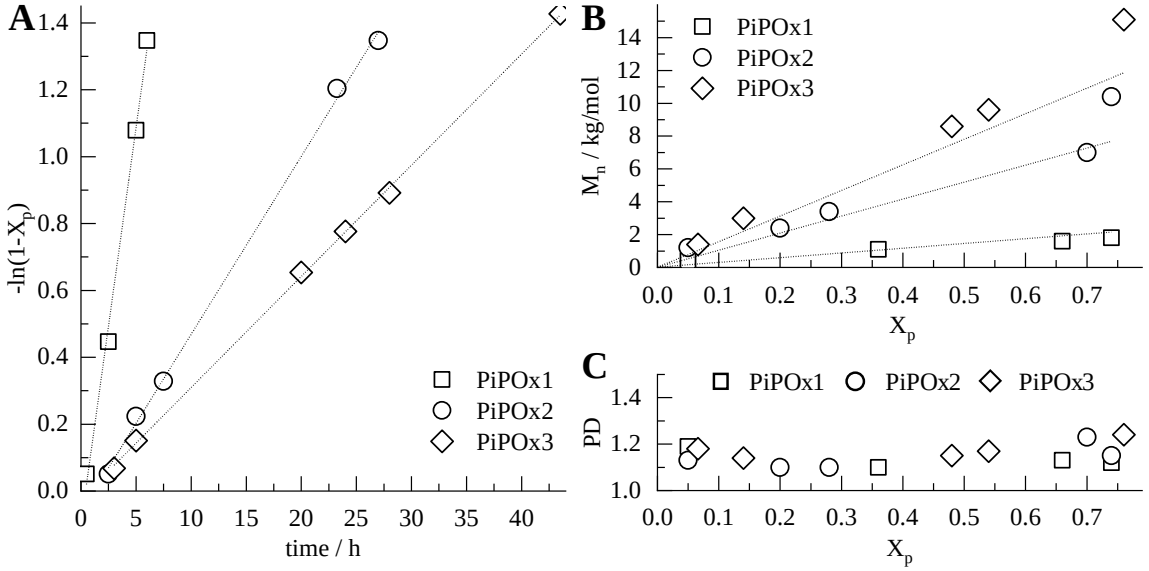

Figure 2 *(A) Semi logarithmic plot of X_p as function of t; (B) Plot of M_n as function of X_p, the dotted lines correspond to the theoretical molecular weights; (C) Polydispersity as function of X_p. M_n and PD obtained from SEC (THF, PS calibration).*

The NMR spectra of the purified PPOxs (Figure 3 A, $CDCl_3$) confirm the purity of the samples. The areas of the resonance signals correspond to the stoichiometry of the respective protons. Proton(s) **b** of each PPOxs exhibit two resonances, separated by 110 Hz (PcyPOx, PiPOx) or 50 Hz (PnPOx). This is due to the existence of different rotational conformers which convert slowly on the NMR time scale. A detailed discussion of the solution properties of the PPOxs follows in section 4.4.

The FT-IR spectra (Figure 3 B) confirm the presence of the azide end group (2100 cm^{-1}). The absorption of the carbonyl stretching vibration (~1630 cm^{-1}) depends on the propyl-substituents.

The molecular weight distributions of the PPOxs were obtained by SEC and MALDI ToF. The absolute M_ns of PiPOx1-3 extracted from the mass spectra are close to the

theoretical molecular weights (Figure 4 A). The M_ns obtained from SEC are larger. This is particularly true for PcyPOx, PnPOx, and PiPOx4 (Figure 4 B).

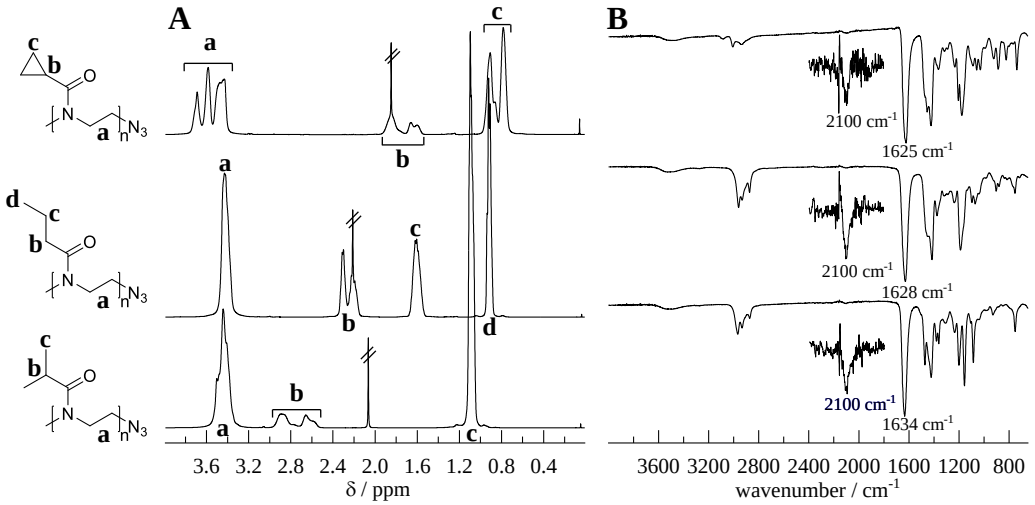

Figure 3 *(A) Assigned ^1H NMR spectra ($CDCl_3$), and (B) FT-IR spectra; (from the top) PcyPOx, PnPOx and PiPOx4.*

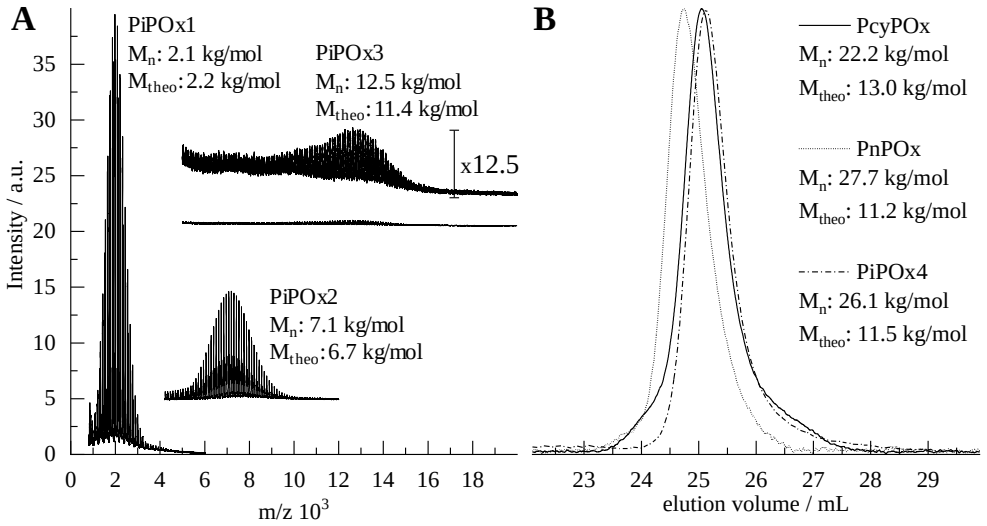

Figure 4 *(A) MALDI ToF mass-spectra of PiPOx1-3; (B) Elugrams of PcyOx, PnPOx, and PiPOx4 (eluent: DMF, PMMA calibration).*

Block copolymers (BCPs) of PiPOx1-3 with PLA were obtained in a two-step procedure. First, lactide (*L*-lactide or *DL*-lactide) was polymerized by ring opening polymerization using propargyl alcohol as initiator. Second, PiPOx and PLA were coupled by azide-alkyne cyclo-addition. A 1.1 molar excess of the azido-functional PiPOx ensured complete conversion of the propargyl-PLA. The unreacted PiPOx was separated from the BCP by centrifugation of an aqueous dispersion. Figure 5 shows the SEC and ^1H NMR data of BCP 3L2, obtained from the coupling of PiPOx3 with PLLA2. The elugrams confirm the success

of the coupling reaction and the removal of unreacted PiPOx3. The disappearance of signals **b** and **e** in the ^{1}H NMR spectrum of 3L2 confirms the completeness of the conversion of the PLLA propargyl end group.

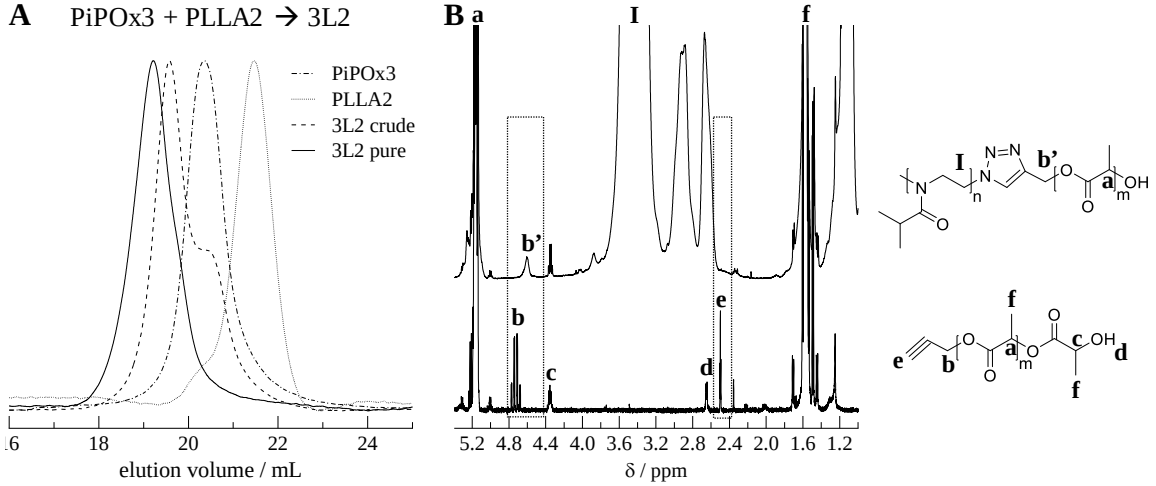

Figure 5 *(A) Elugrams of PiPOx3, PLLA2, 3L2 crude after the coupling reaction, and after purification (eluent: THF); (B) ^{1}H NMR spectra ($CDCl_3$) of (from the bottom) PLLA2, and 3L2 with assignments. Frames highlight the disappearance of signals b and e due to the coupling reaction.*

Table 2 *Molecular properties of the polymers investigated in this thesis.*

Homopolymers				*Diblock copolymers*							
Name	M_n	*PD*	Ref.	Name	*PD*	*n/m*	Φ_{PiPOx}	*N*	M_n	Ref.	Symbol in Fig 11
PLLA1	5.9	1.11	II, III	1L1	1.08	0.30	0.32	81	6.5	II	
PLLA2	10.0	1.09	II, III	1L2	1.08	0.22	0.26	104	8.2	II	□
PLLA3	14.6	1.06	II, III	1L3	1.18	0.15	0.19	141	10.9	II	
PDLLA1	4.9	1.43	II, III	1DL1	1.21	0.27	0.30	87	7.1	II	
PDLLA2	9.0	1.41	II, III	1DL2	1.37	0.20	0.24	112	8.9	II	■
PDLLA3	17.7	1.35	II, III	1DL3	1.37	0.10	0.14	202	15.3	II	
PiPOx1	2.0	1.08	II	2L1	1.03	1.90	0.75	96	9.5	II, III	
PiPOx2	9.3	1.10	II, III	2L2	1.11	1.01	0.62	125	11.6	II, III	○
PiPOx3	15.5	1.28	II, III	2L3	1.08	0.58	0.48	171	14.9	II, III	
PiPOx4*	26.1	1.14	I	2DL1	1.11	1.13	0.64	118	11.1	II, III	
PnPOx*	27.7	1.22	I	2DL2	1.21	0.63	0.50	162	14.3	II, III	●
PcyPOx*	22.2	1.29	I	2DL3	1.29	0.35	0.36	239	19.8	II, III	
PNIPAM*	17.5	1.28	I	3L1	1.10	2.82	0.82	150	15.3	II, III	
				3L2	1.13	1.94	0.75	168	16.6	II	◊
				3L3	1.08	1.04	0.62	217	20.2	II, III	
				3DL1	1.34	1.89	0.75	169	16.7	II, III	
				3DL2	1.33	1.15	0.65	206	19.4	II	♦
				3DL3	1.39	0.61	0.49	292	25.6	II, III	

Table 2 summarizes the molecular properties of all polymers investigated in this thesis. The left hand side contains the homopolymers. The listed *PD* and M_n values were obtained by SEC using as eluent either THF or DMF (the latter marked with an asterisk). The right hand side of Table 2 lists the BCPs. Their name is an acronym built from the respective

homopolymer blocks. The first number stands for PiPOx1, 2 or 3 and the rest of the acronym identifies the PLA block. The *PD* values were obtained from SEC using THF as eluent. The ratio of PiPOx and PLA repeating units, *n/m*, was obtained from the intensities of signals (**I**/4) and (**a**) in the ^{1}H NMR spectra of the BCPs (Figure 5 B). This ratio is used to calculate the molar fraction (not listed) and volume fraction ϕ_{PiPOx}. The degree of polymerization $N=n+m$ in absolute numbers was obtained from the MALDI ToF mass spectra of the PiPOx homopolymers (Figure 4 A) and the molar fraction of PiPOx in the BCPs. The M_n values result also from this calculation.

4.2 Poly(2-propyl-2-oxazoline) solutions

4.2.1 PPOxs in cold water and in cold methanol

PnPOx, PiPOx4 and PcyPOx were investigated by a set of NMR experiments (diffusion ordered NMR, high resolution ^{1}H, NOESY) in cold water and in cold methanol solutions (2.5 wt%) to detect differences of the chain conformation. Table 3 summarizes the results of the NMR experiments with the PPOxs and PNIPAM.

DOSY NMR measurements reveal that the polymer diffusion at 10 °C is faster in methanol than in water in all cases. In water, the R_h values of the polymers are approximately 2.5 times higher than in methanol, which corresponds to an increase of the hydrodynamic volume by a factor of 15. In water, the polymers associate in the form of loose aggregates whereas in methanol they are dissolved as unimers.

Table 3 *Solution properties of the PPOx and PNIPAM polymers in cold water and methanol extracted from NMR experiments*

Polymer	D_{D2O}[1]	D_{CD3OD}[1]	$R_{h,\,D2O}$[2]	$R_{h,\,CD3OD}$[2]	r_{D2O}[3]	r_{CD3OD}[3]
PiPOx4	1.7	9.5	7.3	2.8	0.55:0.5	0.75:0.5
PnPOx	1.9	9.8	6.5	2.7	uniform	0.68:0.5
PcyPOx	1.7	9.2	7.3	2.9	0.66:0.5	0.80:0.5
PNIPAM	2.1	10.4	5.9	2.5	-	-

[1] Diffusion constants in 10^{-11} m^2/s at 10 °C; [2] hydrodynamic radii in nm; [3] ratio on the intensity (area) of the low field to high field signals due the proton(s) H_b, adjacent to the amide carbonyl of the repeat units (see Figure 2).

The slow rotating bonds α and ß (Figure 7 A) can be identified with the help of high resolution ^{1}H NMR spectroscopy. Figure 6 A-C exhibits the spectra of PiPOx4, PnPOx and PcyPOx in D_2O and methanol-d4. Magnifications of the spectral regions around the signals a, due to the methylene protons of the main chain, and b, assigned to the proton(s) adjacent to the carbonyl-carbon are shown in Figure 6 D-F.

The proton H_b adjacent to the double bond appears as two signals corresponding to the "*cis*" and "*trans*" orientations towards the carbonyl-oxygen (Figure 7 B). The two confomers are resolved in the ^{1}H NMR spectra. The ratio r of their populations is given in Table 3. It changes depending on the polymer structure and on the solvent. In water, the rotation is less restricted than in methanol and the populations of the different confomers are more uniform.

The α-bond is part of the delocalized π-electron system of the amide-bond and therefore the two methylene groups bound to same nitrogen-atom are distinguishable in ^{1}H NMR. This situation is analogous to the well understood ^{1}H NMR spectrum of DMF. It exhibits two methyl group signals, one due to the "*cis*" methyl group and the other due to the "*trans*" methyl group with respect to the carbonyl bond. The latter is shifted downfield.[116]

The ^{1}H NMR spectrum of PcyPOx in methanol-d4 exhibits a distinctive pattern of signals. It is schematically explained in Figure 7 B. The signal of H_a in the main chain is split into four resonances of which the two most downfield-shifted ones are assigned to the orientation "*trans*" towards the oxygen. The "trans" and the "*cis*" H_a signals have an intensity ratio of 1:1. The orientation of the proton H_b affects the magnetic environment of the main chain and causes the splitting of the H_a signal into four resonances. The total intensity of the H_a resonances highlighted red and blue in Figure 7 B is four times the intensity of the "*trans*" H_b signal. The same intensity ratio is found for the H_a signals labeled in green and yellow and the "*cis*" H_b signal. The correlation between these protons is further substantiated by Nuclear Overhauser Effect experiments.

It should be noted that all spectra shown in Figure 6, except the spectrum of PnPOx in D_2O, exhibit two separated H_b resonances due to the slow rotation of the ß-bond. The rotation of the PnPOx side-chain in water is not restricted due to its lesser steric demand.

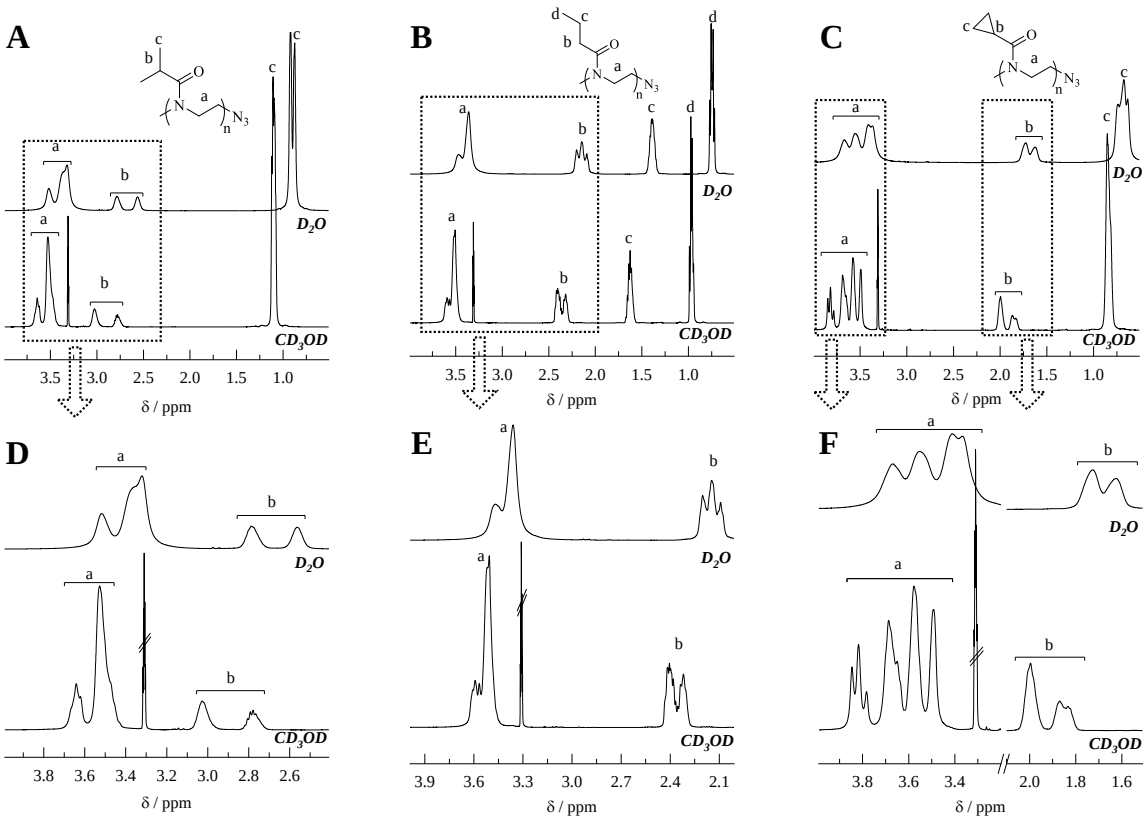

Figure 6 *^{1}H NMR spectra in D_2O and methanol-d4 of (A) PiPOx4, (B) PnPOx, (C) PcyPOx, (D-F) expansions of the spectra above; all spectra are normalized to the intensity of signal a.*

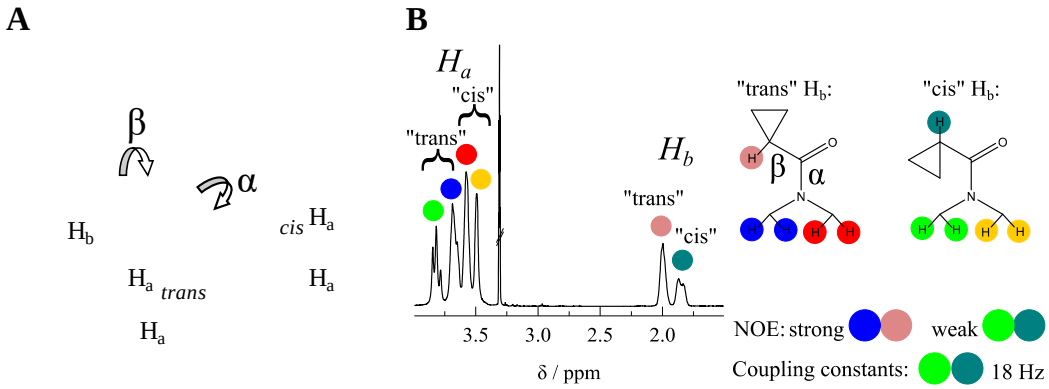

Figure 7 *(A) 3D representation of one repeating unit of PcyPOx highlighting the slow rotating bonds α and ß; (B) assignment of the ^{1}H NMR spectrum of PcyPOx in methanol-d4 with respect to the "trans" and "cis" H_b confomers, "cis" and "trans" of the H_a protons refer to their orientation towards the oxygen atom.*

4.2.2 Temperature dependent properties in water/methanol mixtures

Figure 8 A shows the changes in the solution transmittance of the PPOx samples and PNIPAM solutions in water as a function of temperature. The cloud point temperatures (T_{CP}), defined as the inflection points of the transmittance vs. temperature curves, are given in Table 4. The polymers are soluble in cold water and phase-separate upon heating past the T_{CP} due to the release of polymer-bound water and the collapse of the chain. The transition is reversible by cooling below T_{CP}, which reestablishes the original clarity of the solutions. The release of hydrogen bound water molecules is an endothermic process. The transition enthalpy ΔH is obtained from the area of the endotherms observed by calorimetry (Figure 9).

The aqueous PnPOx solution has the lowest T_{CP} and the highest ΔH values of the polymers investigated. The transition is also the sharpest. This is reflected both in the shape of the turbidity curve and the full width at half maximum (FWHM) of the endotherm (Table 4). The aqueous solution of PcyPOx has a similar T_{CP}, but a low ΔH and a wide transition. The shape of the endotherm of PiPOx4 in water is similar to that of PcyPOx. This is indicative of non-cooperative hydration as a result of the restrained rotations of the side-groups of PcyPOx and PiPOx.

Table 4 *Thermodynamic parameters of the polymer solutions in water*

	PiPOx4	PnPOx	PcyPOx	PNIPAM
$T_{CP,\,H2O}$ / °C	36.0	21.5	23.8	33.9
ΔH_{H2O} / kJ/mol	5.6	6.9	3.2	6.2
$FWHM_{H2O}$ / °C	2.8	1.5	5.1	2.6
$d\Delta H/d\phi_{MeOH}$ / kJ/mol	-0.13	-0.15	-0.08	-0.13

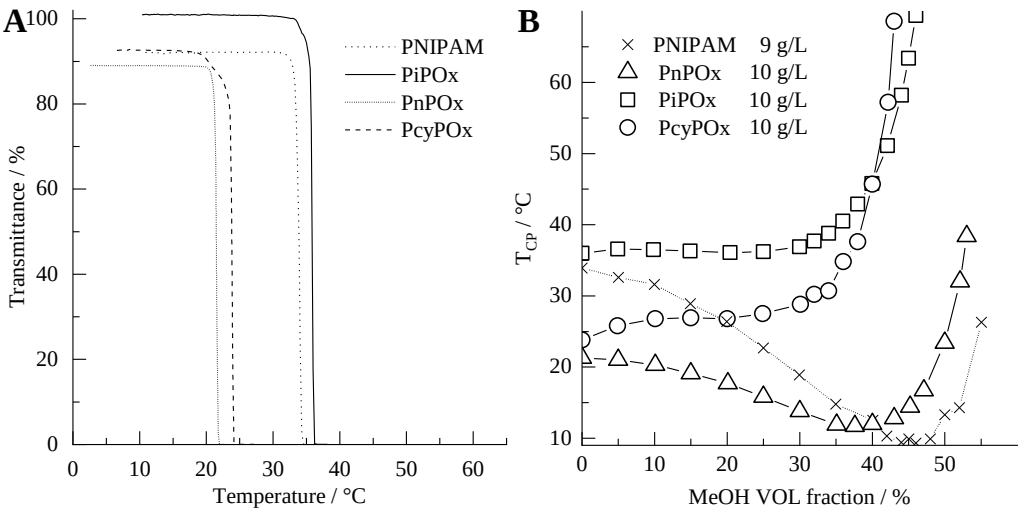

Figure 8 *(A) Transmittance as function of temperature of the PPOx and PNIPAM aqueous solutions during heating; (B) Cloud point temperatures (T_{CP}) of the different polymers in water and water/methanol mixtures of different composition.*

Methanol is a good solvent for the PPOx samples at all temperatures up to the boiling point of the solvent. Figure 8 B presents the T_{CP} values in water/methanol mixtures of the three PPOx samples and PNIPAM. The latter is the classic case of a thermo-responsive polymer exhibiting cononsolvency.[51,52] The sample of PNIPAM in water/methanol mixtures exhibits a decrease in T_{CP} in the composition range of 0 to 45 volume % methanol (Figure 8 B). PnPOx exhibits a behavior similar to that of PNIPAM, although the T_{CP} depression (9.6 °C vs 23.9 °C) is less pronounced in PnPOx. The T_{CP} value of PiPOx4 remains nearly constant up to 20 vol% methanol, increases slowly between 25 and 38 vol% and then increases sharply. The T_{CP} value of PcyPOx increases in the composition range from 0 to 10 vol% methanol, remains constant between 10 and 25 vol% and then increases, similarly to the case of PiPOx4.

Figure 9 shows the thermograms of the PPOx solutions in water/methanol mixtures. Note the different scale of the ordinate in each panel. The methanol content increases from the top to the bottom. For each polymer the transition maxima T_{max} as a function of the methanol content follow the same trends as those observed by the cloud point measurements. Specifically, the thermograms confirm the cononsolvency of PnPOx and the cosolvency of PiPOx and PcyPOx. With increasing methanol content ΔH decreases linearly for each polymer (Figure 10). The slopes of the linear fits are listed in Table 4. The steepest slope is obtained for the series of PnPOx solutions and the flattest slope for PcyPOx.

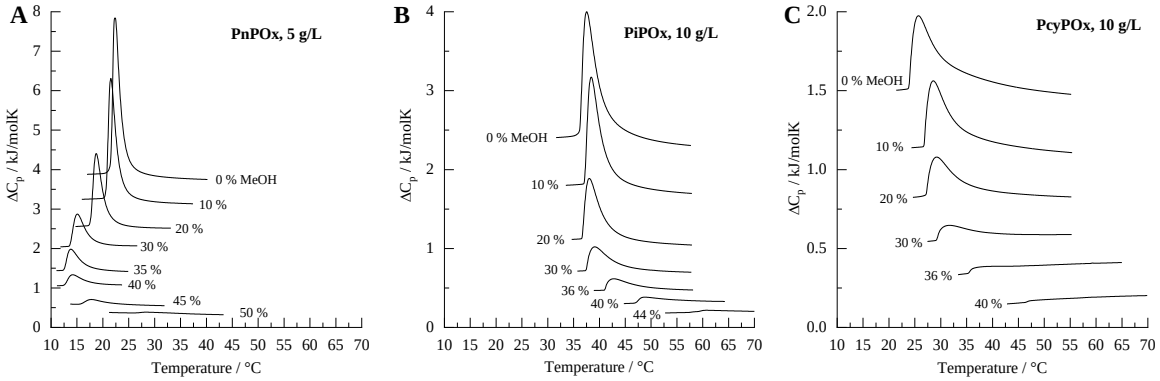

Figure 9 *Thermograms in water/methanol mixtures of (A) PnPOx, (B) PiPOx, and (C) PcyPOx solutions with variable methanol volume fraction.*

The PPOx samples investigated have the tertiary amide moiety in common but they differ in the rotational freedom of the side-groups. From the thermodynamic point of view T_{trans} varies with changes of the ratio $\Delta H/\Delta S$. Figure 10 shows that ΔH decreases linearly with increasing methanol content irrespective of the occurrence of cononsolvency. This leads to the conclusion that the variations in T_{trans} are linked to the entropy term, which consists of contributions of the solvent molecules and the polymer conformation in the coil and globular state. One of the theories assumes that the methanol molecules act as plasticizers for PNIPAM chains collapsed in the globular state.[56,57] This interaction effectively increases the entropy of the globules and tips the enthalpy – entropy balance in favor of the globules. The study of the three PPOx samples brings forward that subtle differences in the polymer structure have unexpectedly strong effects on the phase behavior

in water/methanol solutions that cannot be credited to solely the plasticizing effect of methanol.

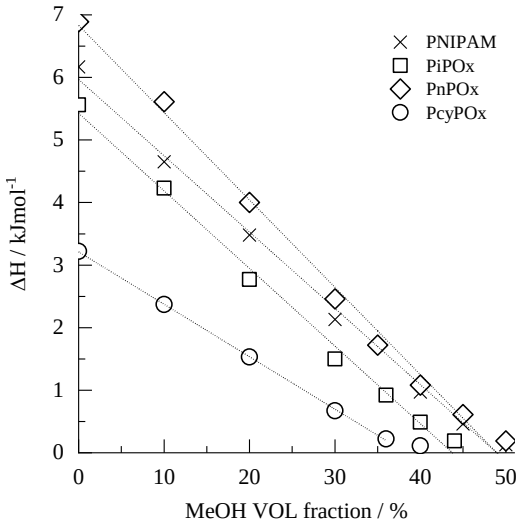

Figure 10 *Transition enthalpy ΔH as function of the methanol volume fraction of the different PPOxs, the lines through the points are linear fits.*

4.3 PiPOx homo- and block copolymers in the bulk

4.3.1 Miscibility of PiPOx and PLA

Figure 11 gives an overview of the BCPs studied in this thesis ordered by the PiPOx volume fraction ϕ_{PiPOx} and the segregation strength χN (Table 2). The calculated interaction parameter χ between PiPOx and PLA repeating units is 0.068, a value that corresponds to a small repulsion between the blocks. The dashed line in Figure 11 is the spinodal predicted for amorphous *A-B* BCPs.[117] Three BCPs are located above this line: 3DL3 (♦), 2DL3 (●) and 3L3 (◊).

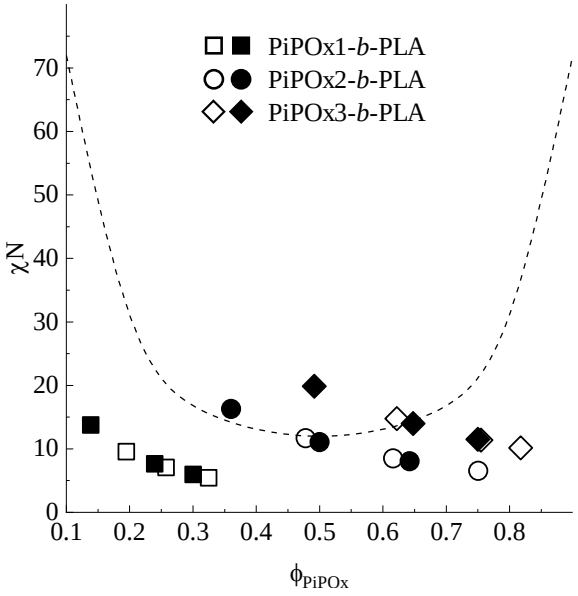

Figure 11 *Overview of the 18 PiPOx-b-PLA BCPs ordered by PiPOx volume fraction ϕ_{PiPOx} and the calculated segregation strength χN. Open symbols correspond to BCPs comprising a PLLA block, closed symbols correspond to BCPs comprising a PDLLA block. The dashed line marks the spinodal line as predicted by Leibler.*[117]

Differential scanning calorimetry (DSC) is the most frequently used experimental technique to detect the miscibility of polymers. A phase separated mixture of polymers exhibits the T_g values of each individual component, while a homogeneous mixture exhibits a single T_g. Domains smaller than 15 nm cannot be resolved by individual T_g transitions in DSC.[118] Figure 12 A shows thermograms in the T_g regions of the homopolymers PiPOx3, PDLLA3, a blend of the two homopolymers and the BCP 3DL3. The T_g values of the pure homopolymers are marked with vertical lines. The blend exhibits two transitions, which are shifted from the values of the pure compounds. Two mixed phases coexist, one is rich in PiPOx3 and the other rich in PDLLA3. The BCP exhibits a single T_g, located between the transitions of the two homopolymers, indicating a single-phase material. The different results of blend and BCP is in agreement with theory. It was discussed earlier that a BCP might be in the homogeneous disordered state, while a corresponding mixture of homopolymers phase separates.[117] The other 17 BCPs showed single T_gs as well (see supporting information of publication I).

To confirm the miscibility of PiPOx and PLA in the BCPs, small angle x-ray scattering (SAXS) of four selected BCPs, 3DL3, 3L3, 1DL1, and 1L1 was measured. The data acquisition was done at 215 °C, above the melting temperature of the polymer. Figure 12 B shows the SAXS scattering curves. There are no Bragg reflections in any of the selected samples. The BCPs are in a disordered state at 215 °C.

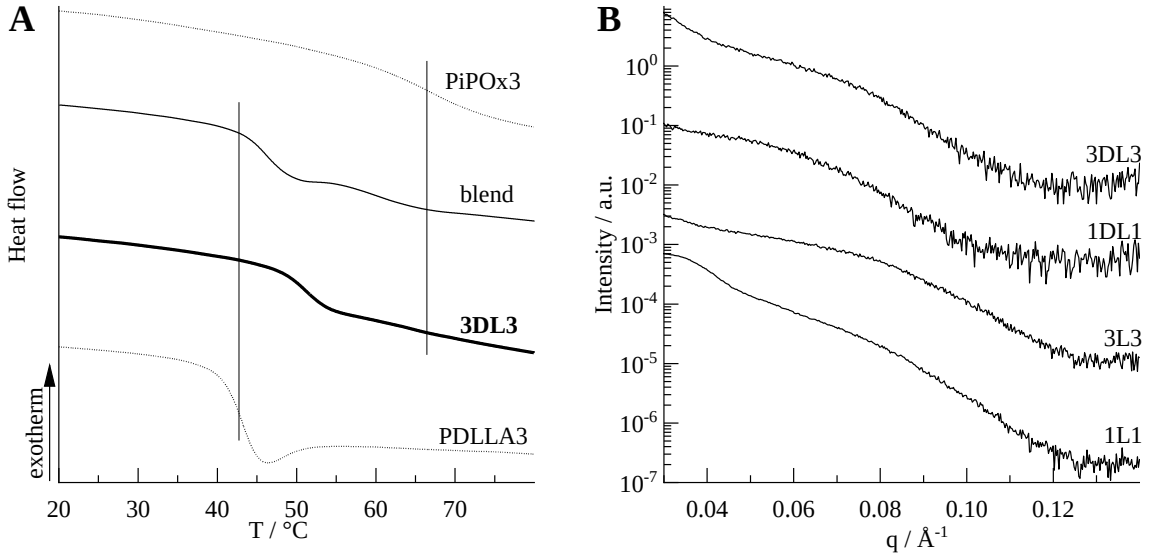

Figure 12 *(A) Thermograms (2nd heating) in the T_g region of PiPOx3, PDLLA3, 3DL3, and a PiPOx3/PDLLA3 blend of the same composition as in 3DL3. Vertical lines mark the T_g of PiPOx3 and of PDLLA3. (B) SAXS curves of selected BCPs at 215 °C.*

The experimental results from DSC and SAXS disagree with Figure 11, in which some BCPs micro-phase separate. This prediction was made based on a calculated interaction parameter. The equation used to calculate the interaction parameter $\chi(T)=\upsilon/RT\cdot(\delta_{PiPOx} - \delta_{PLA})^2$ cannot result in a χ-parameter of negative sign, defined as attractive interactions. However, it is possible that attractive dipolar interactions exist between the carbonyl-groups of PiPOx (amide) and PLA (ester). The amide-carbonyl vibration in the FT-IR spectra of PiPOx1 (1634 cm^{-1}) and 1L3 (1643 cm^{-1}) is shifted by 9 cm^{-1} in the presence of PLLA, indicative of a significant change of the polarization of this bond.

4.3.2 Crystallization behavior

4.3.2.1 Homopolymers

The equilibrium melting temperature, $T_m°$, of the homopolymers was determined by recording the dependence of T_m as function of T_c (Figure 13 A). The polymer melt was cooled rapidly to a temperature above T_g and kept at the same temperature until crystallization was complete (2 hours). Subsequently, the polymer was heated and the onset of melting recorded. $T_m°$ is the intersection of the extrapolated T_m vs T_c data points with the virtual line $T_m = T_c$, at which crystallization and melting processes cancel each other. The $T_m°$ values of three PiPOx (2 - 15 kg/mol) and three PLLA (6 - 15 kg/mol) homopolymers are listed in Table 5. For PLLA, $T_m°$ increases with molecular weight from 156 to 183 °C, while for PiPOx1 $T_m°$ is 149 °C and for PiPOx2 and PiPOx3 it is nearly identical (~205 °C).

Table 5 *Equilibrium melting temperature T_m° and inverse crystallization half time $\tau_{1/2}^{-1}$ at a T_c of 130 °C of the homopolymers*

	PiPOx1	PiPOx2	PiPOx3	PLLA1	PLLA2	PLLA3
T_m° / °C	149	203	205	156	178	183
$\tau_{1/2}^{-1}$ / min^{-1}	-	0.08	0.11	0.03	0.56	0.73

Isothermal crystallization provides also information on the crystallization kinetics. We determined the time until half of the exothermal crystallization event was completed (Figure 13 B). The inverse of these values ($\tau_{1/2}^{-1}$) were plotted as a function of T_c (Figure 13 C). As an example, the $\tau_{1/2}^{-1}$ values for PiPOx and PLLA homopolymers at T_c 130 °C are given in Table 5. Ideally, one should obtain a bell-shaped curve, with low $\tau_{1/2}^{-1}$ values near T_m° and T_g. For PLLA, the crystallization rate determining factor is the intrinsic viscosity.[119] The highest recorded $\tau_{1/2}^{-1}$ value increases with decreasing molecular weight. For PiPOx, the highest $\tau_{1/2}^{-1}$ values are considerably lower than for PLLA and increase with increasing molecular weight. This indicates that for PiPOx the chain mobility is not the crystallization rate determining factor. The crystallization of PiPOx is directed by oriented dipolar interactions[63] and requires concerted main-chain and side-chain conformational changes.[65,120] With increasing PiPOx molecular weight, the number of oriented dipoles per chain increases which might result in increasing crystallization rates.

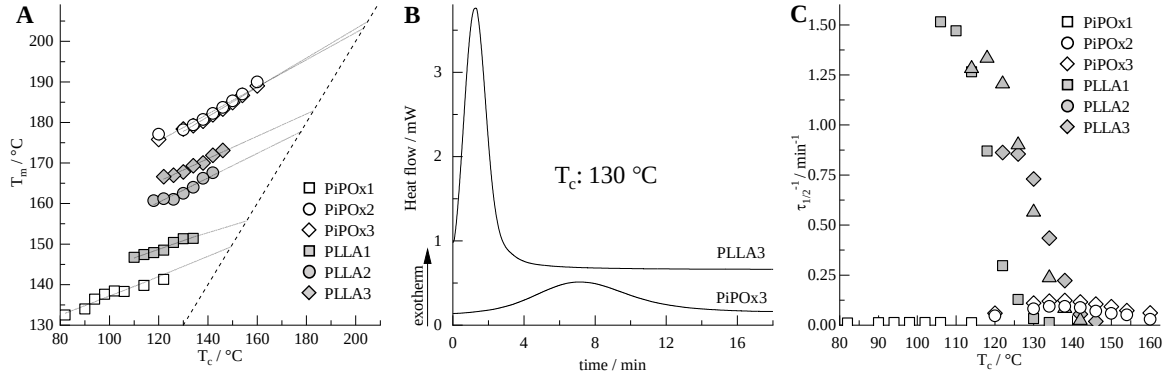

Figure 13 *(A) Melting temperatures T_m as function of T_c of the homopolymers; (B) Crystallization isotherms at 130 °C of PiPOx3 and PLLA3; (C) Inverse crystallization half-times $\tau_{1/2}^{-1}$ as function of the crystallization temperature T_c of the homopolymers PiPOx1, 2, 3 and PLLA1, 2, 3.*

Figure 14 shows photographs taken while monitoring by polarized optical microscopy the isothermal crystallization at 130 °C of several samples. The samples were cooled from the isotropic melt. Frames A and B show the different crystalline superstructures of PLLA3 and PiPOx3, respectively. PLLA3 started to crystallize immediately when the sample reached 130 °C and spherulites filled the entire sample area within 5 min (radius: 430 µm +/- 100 µm). PiPOx3 crystallized in a granular superstructure (radius: 35 µm +/- 5 µm). The first granules appeared after 12 min and it took 45 min until no further changes were detectable.

Frame C of Figure 14 shows the crystalline superstructures of a PiPOx3/PLLA3 blend with the same composition as the BCP 3L3. Both granules and spherulites are visible. The first superstructure to be seen were granules of PiPOx after 8.5 min followed by few spherulites after 15 min. The radius of the spherulites increased to 1200 µm +/- 400 µm.

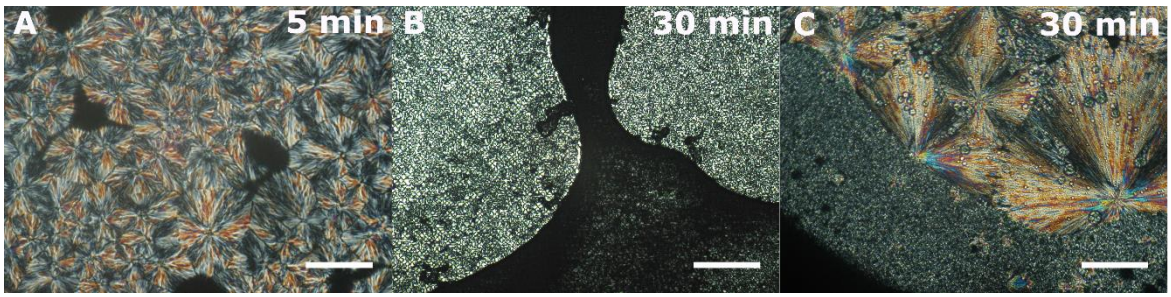

Figure 14 *Polarized optical microscopy images taken during the isothermal crystallization at 130 °C. The elapsed time after reaching T_c is indicated in the top right corner of each frame. Scale bar: 1 mm; (A) PLLA3; (B) PiPOx3; (C) PiPOx3/PLLA3 blend.*

4.3.2.2 Block copolymers

Figure 15 shows photographs after 30 min of isothermal crystallization at 130 °C of the BCPs 3L3, 2L3 and 1L3 obtained by polarized optical microscopy. Frames A and B exhibit only granular superstructures, which appeared after 6.5 min and 3 min, respectively. In frame C (1L3) only spherulites are visible. They appeared 1 min after reaching 130 °C and it took 90 min to convert the isotropic melt into the crystalline state.

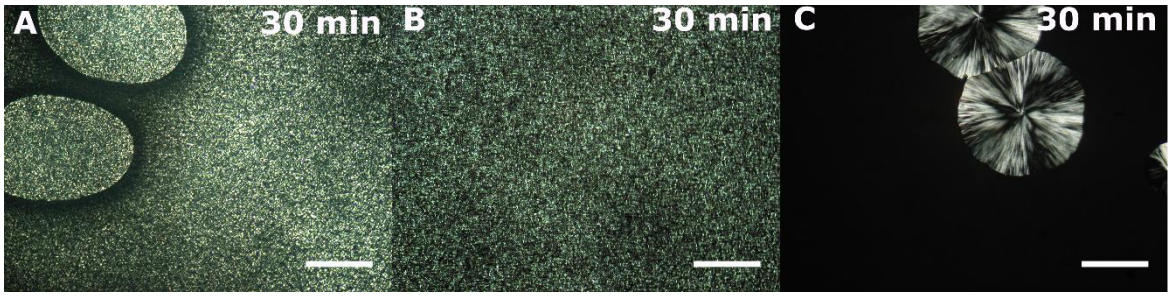

Figure 15 *Polarized optical microscopy images taken during the isothermal crystallization at 130 °C. The elapsed time after reaching T_c is indicated in the top right corner of each frame. Scale bar: 1 mm; (A) 3L3; (B) 2L3; (C) 1L3.*

The crystal structures of the homo- and block copolymers after 2 hours of isothermal crystallization at 130 °C were investigated by WAXS (Figure 16 A). The amorphous PiPOx1 exhibits no sharp signals. PiPOx3 and PLLA3 crystallized in their well-known crystal structures.[83,121] The selected BCPs exhibit different features in the WAXS curves. 3L3 exhibits only the signals of crystalline PiPOx, 1L3 only those of crystalline PLLA,

while 2L3 is the only double-crystalline BCP of the entire library. 1L1 is amorphous. These results were confirmed by the melting endotherms recorded after isothermal crystallization (Figure 16 B). The thermogram of 3L3 exhibits only the melting of PiPOx, while that of 2L3 contains two endotherms, one at the characteristic T_m of PLLA the other at the T_m of PiPOx. The thermogram of 1L3 shows the double melting peak of PLLA due to crystallites of different size.

Figure 16 C presents the inverse crystallization half times $\tau_{1/2}^{-1}$ at 130 °C of all BCPs that were detectable by crystallization. The $\tau_{1/2}^{-1}$ value of 1L3 is drastically lower than that of PLLA3 (0.73 min^{-1}). In contrast, the $\tau_{1/2}^{-1}$ values of PiPOx in the BCPs increase, compared to the homopolymers PiPOx2 (0.08 min^{-1}) and PiPOx3 (0.11 min^{-1}).

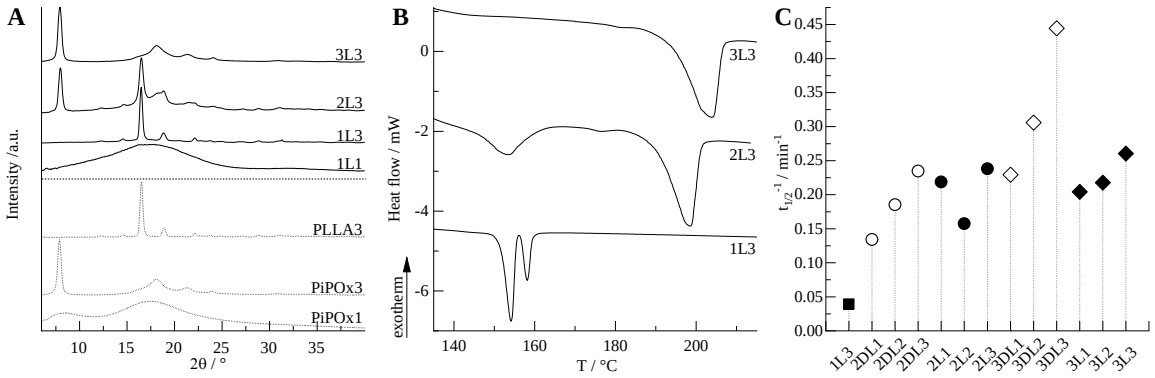

Figure 16 *(A) Wide angle x-ray scattering curves of various homopolymers (···) and BCPs (–) after isothermal crystallization at 130 °C for 2 hours; (B) Thermograms (10 °C/min) of selected BCPs after isothermal crystallization at 130 °C for 2 hours; (C) Inverse crystallization half times $\tau_{1/2}^{-1}$ at a T_c of 130 °C of the BCPs.*

The PiPOx-*b*-PLA block copolymers form a disordered isotropic melt. The PLA block separates the PiPOx amide-dipoles. This plasticization effect facilitates the rearrangements of the PiPOx chains before crystallization can take place. The crystalline PiPOx phase of the BCP samples is indistinguishable on the atomic level (WAXS) from the crystalline phase of PiPOx homopolymers, indicating that the crystallization of PiPOx causes the BCPs to micro-phase separate. The crystallization of PLLA, which requires mobile polymer chains and a high PLLA concentration near the crystallization nuclei is hindered in the presence of PiPOx. The same processes take place in the PiPOx/PLLA blend causing an increase of the crystallization rate of PiPOx and a reduction of the crystallization rate of PLLA. However, as PLLA can migrate independently from regions of crystalline PiPOx, PLLA rich domains are formed and eventually they crystallize in the sperulitic superstructure.

4.4 Aqueous dispersions of PiPOx-*b*-PLA

4.4.1 Particle morphology

Particle dispersions were prepared by adding a solution of PiPOx-*b*-PLA in tetrahydrofuran (THF) to water, followed by removal of the organic solvent. PLA is insoluble in water and forms a dispersed phase. During the self-assembly process an interesting situation arises: PiPOx can locate either in the continuous phase (water) or in the dispersed phase. In the first case PiPOx and PLA would micro-phase separate and form a particle of core-shell morphology, as observed for example in the case of PEG-*b*-PLA. In the other case PiPOx and PLA would mix and combine.

Figure 17 A shows a cryo-TEM image of a dispersion of 3L3 subjected to vitrification at room temperature immediately after the preparation. The contrast of the particles against the vitrified water was not enhanced by staining the sample. The image shows fuzzy objects with a radius of 8.7 +/- 1.4 nm, one of which is highlighted with an arrow. The distance to the nearest neighbors measured from center to center is 70 +/- 10 nm, which is approximately twice the hydrodynamic radius R_h of the particles (39 nm) obtained by dynamic light scattering (DLS). The regular distance between the objects is due to steric repulsion. The low contrast indicates a low density of the particles, which decreases from the center to the surface. Only the most central part of the particles can be captured by cryo-TEM.

To distinguish whether PiPOx micro-phase separates or mixes with the PLA phase ^{1}H NMR spectra of the dispersions in D_2O are compared to the spectrum of a PiPOx solution in D_2O (Figure 17 B). The concentration of PiPOx in the solution spectrum and the dispersion spectra is similar. The spectra are normalized to the intensity of the HOD signal. The intensity of the PiPOx signals in the dispersion spectra is reduced by a factor of 400 (2L2) and 150 (3DL3) compared to the solution spectrum. The signals of the PLA blocks are not observed in the spectra of the dispersions due to their low mobility. The spectra imply that in the dispersions most of the PiPOx chains are immobile on the NMR time scale and do not form a solvated shell around the particle core. The residual PiPOx signals become visible after enhancing the intensity of the spectra by a factor of 75. This indicates that the 3DL3 dispersion has a larger fraction of mobile PiPOx chains than the 2L2 dispersion. It should be noted, that in ^{1}H NMR spectra of dispersions of PEG-*b*-PLA in water the intensity of the PEG signal is not reduced signaling that PEG-*b*-PLA adopts a core-shell morphology, unlike PiPOx-*b*-PLA.[122,123]

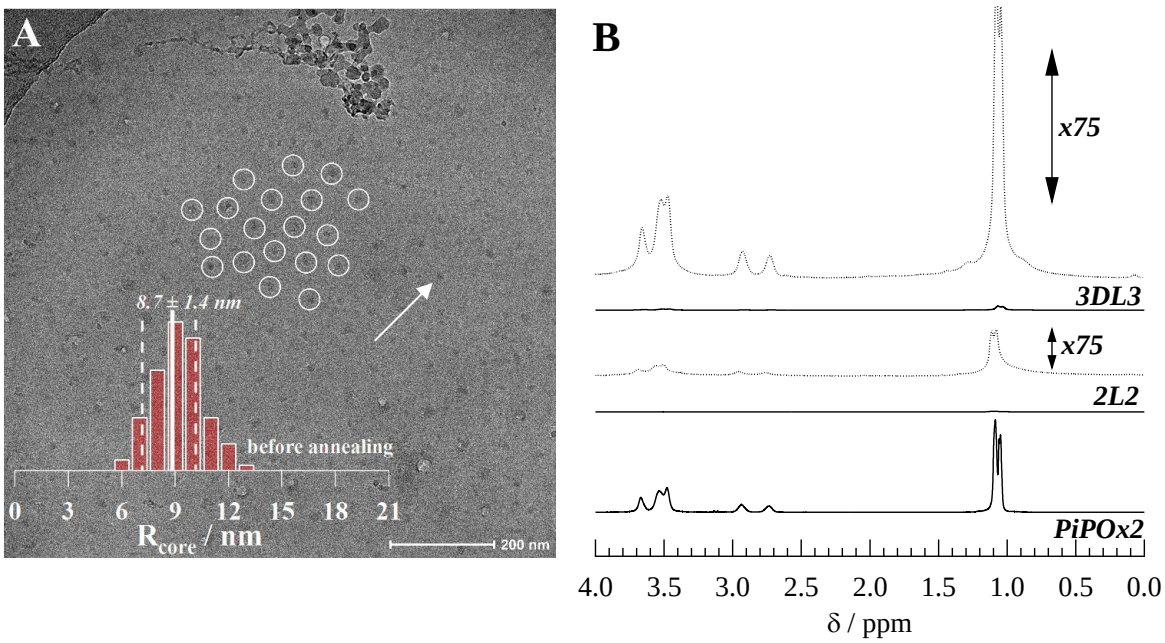

Figure 17 *(A) Cryo-TEM image of a 3L3 dispersion (0.5 g/L) vitrified at room temperature immediately after preparation. The inset shows a histogram of the particle core radius. (B) ^{1}H NMR spectra in D_2O at room temperature of a PiPOx2 solution (10 g/L), a 2L2 dispersion (25 g/L) and a 3DL3 dispersion (25 g/L). The solid lines are spectra normalized to the HOD signal (4.8 ppm). The dotted lines are intensity enhanced spectra (x75) of the dispersions.*

The particle dispersions were analyzed at 20 °C immediately after preparation by combined dynamic and static light scattering (DLS and SLS) at various angles. Plots of the decay rates Γ vs. the squared scattering vector q exhibit translational diffusion of the particles (Figure 18 A). The R_h values were obtained from a linear fit to the data. They are listed in Table 6. The R_h of the particles increases with the molecular weight and ranges between 18 and 60 nm. The respective CONTIN plots (Figure 18 B) exhibit rather broad size distributions for some of the dispersions. The particle form factor $P(q)$ is the ratio of Rayleigh ratio at the scattering vector q, divided by the extrapolated Rayleigh ratio at $q = 0$. The fit of the exponential decay of $P(q)$ as function of q^2, known as Guinier plot, gives the radius of gyration (R_g) of an homogeneous sphere (Figure 18 C and Table 6). R_g increases with molecular weight. The ratio $\rho = R_g/R_h$ is indicative of the mass distribution and particle morphology. The theoretical values of ρ for homogeneous hard spheres and for monodisperse random coils are 0.775 and 1.50, respectively.[124] A value of 0.926 is predicted for solvent permeable globules with uniform segment density.[125] The dispersions of PiPOx-*b*-PLA exhibit a ρ-value between 0.9 and 1.1, except in the case of the dispersion of 2DL1 (1.6). This is remarkable since the PiPOx volume fraction ϕ_{PiPOx} of particles with the same ρ parameter ranges from 0.36 (2DL3) to 0.82 (3L1). The similar ρ parameters listed in Table 6 indicate that the PiPOx-*b*-PLA particle structure is invariable to variations of the hydrophilic-to-hydrophobic fraction. The particle size distribution of the 2L3 dispersion is constant for at least 20 days when the sample is kept at room temperature.

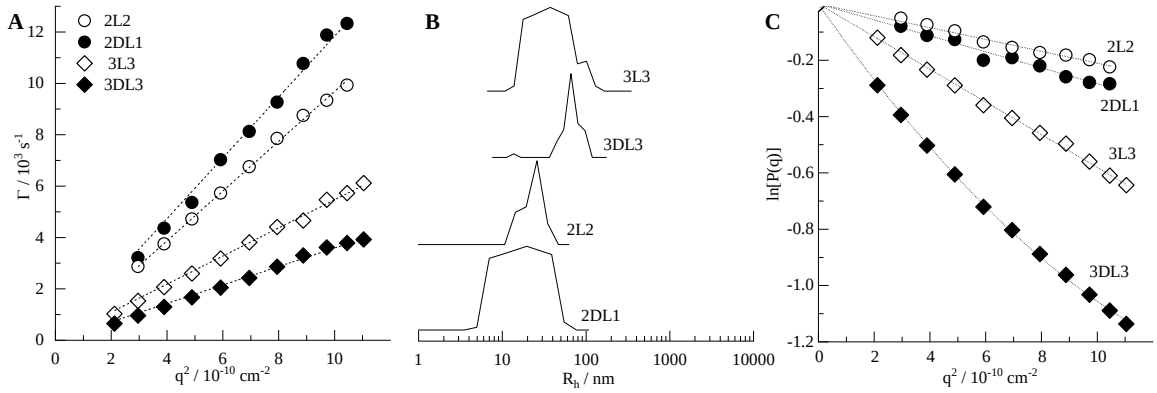

Figure 18 *(A) Decay rates Γ as function of the squared scattering vector q of selected BCP dispersions (0.5 g/L) in water obtained by dynamic light scattering; (B) Unweighted particle size distributions obtained by CONTIN analysis of the autocorrelation functions detected at a scattering angle of 90 °; (C) Guinier fits of the form factor P(q) as function of q^2.*

Table 6 *Particle properties at 20 °C obtained by light and small angle neutron scattering of dispersions as prepared and after keeping at 50 °C for 2 hours.*

	As prepared					*After 2 h at 50 °C*			
Name	R_h[a]	<Poly>[b]	R_g[c]	R_g/R_h	R^{SANS}	R_h[a]	R_g[c]	R_g/R_h	R^{SANS}
2L1	19	0.21	20	1.0	-	-	-	-	-
2L2	**22**	**0.17**	**25**	**1.1**	**15.1**	**24**	**24**	**1.0**	**15.3**
2L3	28	0.23	31	1.1	-	-	-	-	-
2DL1	**18**	**0.23**	**29**	**1.6**	**9.9**		**bimodal**		**9.2**
2DL2	29	0.19	28	0.9	-	-	-	-	-
2DL3	39	0.15	39*	1.0	-	-	-	-	-
3L1	22	0.16	22	1.0	-	-	-	-	-
3L3	**39**	**0.21**	**42**	**1.1**	**17.5[d]**		**bimodal**		**16.1[d]**
3DL1	25	0.22	28	1.1	-	-	-	-	-
3DL3	**60**	**0.13**	**65***	**1.1**	**17.3**		**bimodal**		**14.0**

All radii are given in nm; [a] Hydrodynamic radius R_h is obtained by the linear fit to the data presented in Figure 3 A. [b] Averaged particle dispersity is obtained from 2nd order cumulant analysis at 11 scattering angles. [c] Radius of gyration R_g is obtained by a fit of first or second order (marked with an *) to the ln[$P(q)$] vs q^2 data presented in the SI of III. [d] core-shell model with 12.0 nm core and 5.5 nm shell before heating and 13.3 nm core and 2.8 nm shell after heating.

Dispersions of 2L2, 2DL1, 3L3 (all ϕ_{PiPOx}: ~0.6) and 3DL3 (ϕ_{PiPOx}: 0.5) in D_2O were analyzed at 20 °C by small angle neutron scattering (SANS). A model independent Guinier fit of the data taken from the 2L2 dispersion gives an R_g value of 14.8 nm. The scattering intensities as function of q are fitted with models representing homogeneous spheres (2L2, 2DL1 and 3DL3) or a core-shell structure (3L3) (Figure 19). The latter is necessarily due to

a bad fit of the data with the homogeneous sphere model, resulting from the higher density of the central region of the 3L3 particles. The radii resulting from the SANS data are smaller than those obtained by light scattering (Table 6). In SANS the scattering contrast is given by the difference between the scattering length densities of the dispersed and the continuous phase. The contrast of the dispersed phase is low when it is solvated. The analysis of the SANS data of dispersions of 2L2, 3L3 and 3DL3 gives similar radii. In comparison, there are significant differences in size between the samples observed by light scattering. However, the ρ parameters of the samples are constant (1.1). Taken together this indicates that the morphologies of 2L2, 3L3 and 3DL3 particles are similar. The spherical objects are permeated by substantial amounts of solvent, which leads to a cut-off radius for SANS observations of 15 -18 nm. The particles of 2DL1 are more hydrated leading to a smaller R^{SANS} value and a higher ρ parameter compared to the other samples.

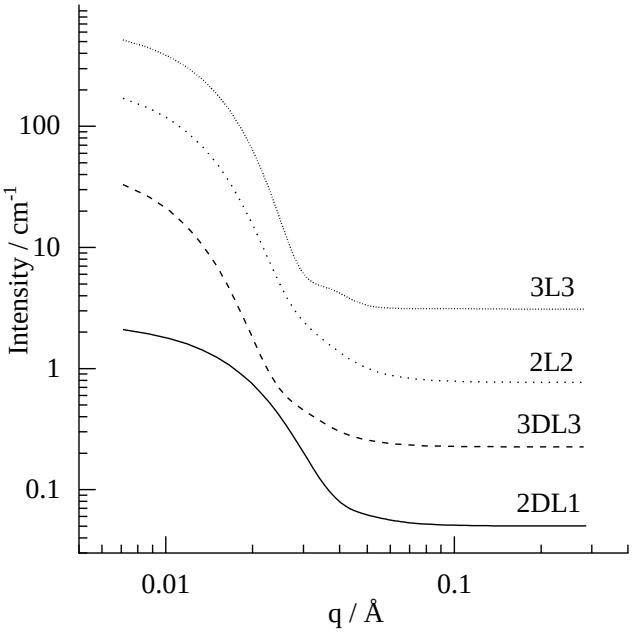

Figure 19 *Fits to the SANS data of selected dispersions in D_2O (5 g/L) at 20 °C obtained immediately after particle preparation. Note that the lines were shifted vertically.*

4.4.2 Temperature dependent behavior

Figure 20 A and B show the transmittance of the aqueous particle dispersions as function of temperature during heating and cooling, respectively. The T_{CP}s taken from transmittance measurements of homopolymer solutions in water (PiPOx2 and PiPOx3) are listed in Table 7. The curves of the homopolymer solutions exhibit a sharp transition from 100 % to 0 % transmittance as discussed in section 4.2.2. The dispersion of 2L2 exhibits no changes in transmittance in the entire temperature range during heating and cooling. A similar result is obtained for the dispersion of 3L3. During cooling, this sample exhibits a slight decrease of transmittance between 80 °C and 45 °C from 100 % to ~70 %. The transmittance of the 2DL1 dispersion exhibits a minor change at 38 °C and then decreases with increasing rate at temperatures above 53 °C. This process continues during cooling until the temperature

falls below 58 °C. At 37 °C the transmittance increases slightly but the initial clarity of the dispersion is never reestablished. The 3DL3 dispersion exhibits a sharp decrease of transmittance at 43 °C, similar to the homopolymer solution. The dispersion remains turbid after cooling.

Thermograms of the four dispersions are shown in Figure 20 C. In all cases the transition enthalpies are low compared to the homopolymer solutions (Table 7). The dispersions of 2L2 and 3L3 exhibit broad transitions with a peak at low temperatures and a shoulder near the temperature of the homopolymer transition. The dispersion of 2DL1 exhibits two baseline separated low and high temperature transitions corresponding to the temperatures at which changes of the transmittance occurred. The thermogram of the 3DL3 dispersion exhibits a low temperature shoulder and high temperature peak.

The thermo-responsive behavior of PiPOx-*b*-PLA dispersions observed by transmittance and calorimetric measurements is strikingly different from that of the homopolymer solutions. The transitions are non-cooperative and the enthalpies are low. The transmittance responds very weakly if at all. These observations support the hypothesis of a dispersed phase in which PiPOx and PLA mix. In comparison micelles consisting of a polyion complex core and a phase separated PiPOx corona exhibited sharp thermal transitions.[113]

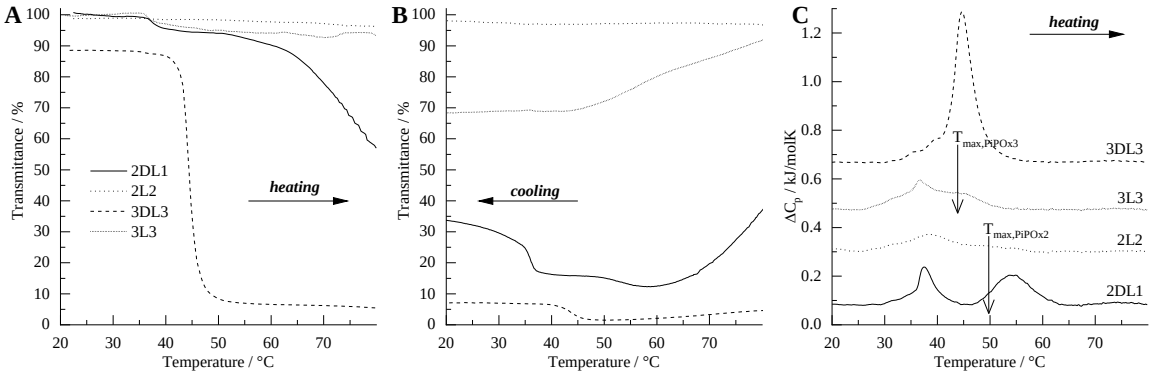

Figure 20 *Dispersion transmittance during (A) heating and (B) cooling; (C) Thermograms of the dispersions during heating, arrows mark the transition maximum of the respective PiPOx homopolymer solutions. The polymer concentration of the dispersions was 0.5 g/L.*

Table 7 *Thermal properties of PiPOx solutions and dispersions*

	polymer	c_{PiPOx}[a]	T_{CP}[b]	T_{low}[c]	T_{high}[c]	ΔH_{low}[d]	ΔH_{high}[d]
solutions	PiPOx2	0.30	45.9		49.6		4.8
	PiPOx3	0.30	41.4		43.6		4.8
dispersions	2L2	0.31		38.4	48.8	0.8	
	3L3	0.31		36.6	45.0	1.4	
	2DL1	0.32		37.4	53.5	0.6	0.9
	3DL3	0.25	42.7	39.1	44.7	3.5	

[a] In g/L, nominal PiPOx concentration of the sample. [b] In °C, cloud point temperature from turbidimetry. [c] In °C, shoulder or maximum in the thermograms. [d] In kJ/mol, transition enthalpy with an error margin of +/- 0.1 kJ/mol.

The transmittance measurements of the dispersions of 3L3, 2DL1 and 3DL3 indicated irreversible processes at elevated temperatures. Figure 21 shows particle size distributions obtained by DLS analysis of a 3L3 dispersion at different temperatures. The average R_h is 49 nm at 20 °C and decreases to 40 nm at 42 °C, a temperature in the middle of the transition observed by µDSC. At 51 °C, which is above the calorimetric transition, the size distribution becomes bimodal (~30 nm and ~200 nm). After cooling back to 20 °C the bimodality is retained and both populations are larger compared to the sizes at 50 °C (~45 nm and ~420 nm).

Table 6 lists the properties of the dispersions after keeping them at 50 °C for 2 hours and cooling them to 20 °C. DLS gives bimodal distributions of the dispersions of 3L3, 2DL1 and 3DL3. At elevated temperature the particles form clusters, which retain their aggregated state after cooling below the T_{CP} of PiPOx. The dispersion of 2L2 is stable against aggregation at elevated temperature and no changes of R_h and R_g are observed after heating. The radii of the heat-treated samples, obtained by SANS, are similar to the radii before heating. Clusters larger than 100 nm are out of the size range observable by SANS. However, the SANS data reveal differences of the 3L3 dispersion before and after heating (Figure 21). After heating the best fit was obtained with a cylindrical core-shell model, which suggests a directional growth of the clusters. WAXS data before and after heating the 3L3 dispersion are identical and confirm that the temperature induced transformations are not driven by crystallization. In comparison, no transformations of the particles are detected by SANS and light scattering for the dispersion of 2L2 after the heat treatment.

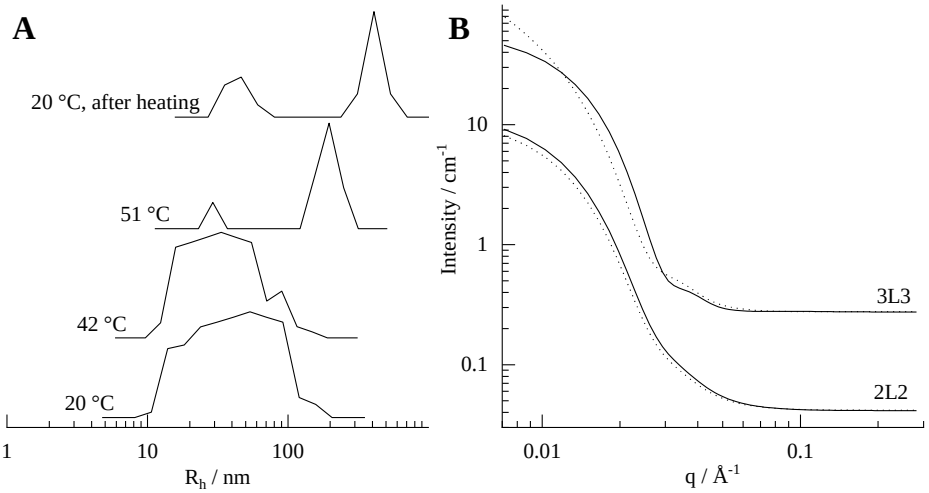

Figure 21 *(A) Particle size distributions of the 3L3 dispersion at different temperatures (0.5 g/L, 60 ° scattering angel); (B) Fits to the SANS data of dispersions of 2L2 and 3L3 at 20 °C (—) before heating and (···) after keeping at 50 °C for 2 hours.*

Scheme 5 illustrates the particle morphologies of four different dispersions based on the analysis of ^{1}H NMR spectra, cryo-TEM, light scattering, SANS and the thermo-responsive

behavior. Taken together all results support the model of a dispersed phase consisting of a mixture of PiPOx and PLA. The dispersed phase is permeated by the solvent. The molecular weight of the blocks and the PLA stereochemistry influence the particle morphology and the thermo-responsive behavior. Particles consisting of PiPOx-*b*-PLLA are less permeable by water and form denser particles compared to PiPOx-*b*-PDLLA. Loops and tails of PiPOx orient towards the particle surface and stabilize the dispersions. These chains are divided in short segments and their dehydration is non-cooperative. It is well documented that the T_{CP} of aqueous PiPOx solutions depends on the molecular weight. Oligomers consisting of six repeating units are permanently water soluble.[37,43,44]

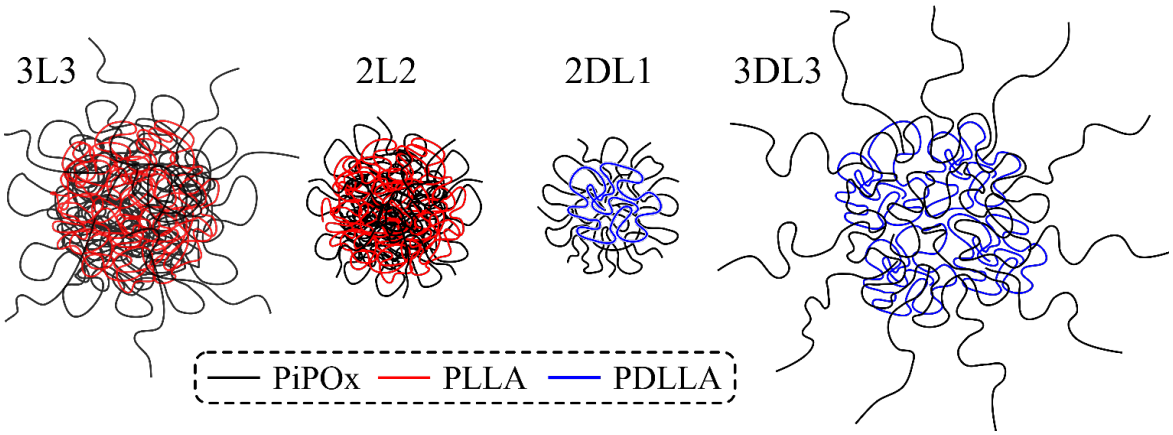

Scheme 5 *Particle morphology of PiPOx-b-PLA dispersions in water.*

5 Conclusion

Poly(2-propyl-2-oxazoline)s were synthesized by cationic ring opening polymerization and terminated with an azide end-group. The molecular weight of the homopolymers ranged from 2 kg/mol to 12 kg/mol (MALDI-ToF) and was controlled by the monomer-to-initiator ratio. The obtained polymers were narrowly dispersed (SEC) and their structure was analyzed by NMR- and FT IR-spectroscopy. Poly(lactide) was prepared by ring opening polymerization yielding a linear polymer with an alkyne end-group. Block copolymers (BCP) of poly(2-isopropyl-2-oxazoline) (PiPOx) and poly(lactide) (PLA) were obtained by click coupling. The volume fraction of PiPOx in the PiPOx-*b*-PLA BCPs ranged from 14 to 82 %.

PnPOx, PiPOx and PcyPOx are soluble in cold water and in methanol at all temperatures. NMR spectroscopy reveals important information on the solution properties. In methanol the PPOxs dissolve as unimers, whereas in water they form loose clusters. PnPOx in cold water exhibits free rotation of the n-propyl side-group but the rotation is limited in methanol. In contrast, the rotation is hindered for solutions of PcyPOx and PiPOx in water and in methanol. This affects the hydration cooperativity and the collapse transition observed by transmittance measurements and calorimetry. The phase diagrams constructed in water/methanol mixtures of variable composition reveal important differences: PnPOx exhibits cononsolvency, PcyPOx and PiPOx cosolvency. The transition enthalpy decreases linearly with increasing methanol content, irrespective of the changes of the transition temperature. These findings shed light on the influence of the polymer structure on the delicate balance of entropy and enthalpy of mixing and their contributions to the free energy of mixing in ternary polymer solutions.

The bulk phase behavior study was performed for PiPOx, PLA, their blends, and PiPOx-*b*-PLA BCPs. This part of the study focused, first, on the miscibility of PiPOx and PLA and, second, on the influence of miscibility on the polymers' crystallization behavior. PiPOx-*b*-PLA BCPs form a homogeneous melt (SAXS) and exhibit a single glass transition. A shift of the PiPOx carbonyl-stretching vibration (FT-IR) indicates the existence of dipole-dipole-interactions between the PiPOx and PLA blocks. These findings are further supported by the similar solubility parameters of PiPOx and PLA. PLA acts as a plasticizer of PiPOx: the crystallization rates of PiPOx in the BCP samples are significantly faster than that of the homopolymers (polarized optical microscopy, calorimetry). This goes at the expense of the crystallization of PLLA, which remains amorphous in most of the samples. Only one double crystalline PiPOx-*b*-PLLA sample was observed (WAXS). The crystallization properties depend on the molecular weight and the volume fractions of the blocks.

Aqueous PiPOx-*b*-PLA dispersions were prepared by transferring the BCPs from a common solvent (THF) to a non-solvent for PLA (water). In this situation water competes with PLA for the interactions with PiPOx. The dispersed phase consists of a mixture of PiPOx and PLA. A small fraction of PiPOx chains orient towards the particles surface and the continuous water phase (NMR). The particles are permeated by water molecules and the contrast in cryo-TEM and SANS is low. The mass distribution within the particles is constant over a wide range of PiPOx volume fraction: the R_g/R_h ratio is close to unity for most of the samples (light scattering). Due to the interaction of PiPOx and PLA short

segments of PiPOx remain tethered to the particle surface and stabilize the particles. The response of these segments to changes in the dispersions' temperature is non-cooperative and strikingly different from that of PiPOx homopolymers. The transmittance changes slowly upon heating and the endotherm is broad. The transition enthalpy is low due to the small fraction of PiPOx undergoing a collapse transition. Changes of the transmittance are irreversible due to the irreversible aggregation of the particles at elevated temperature. At room temperature the particles are colloidally stable for extended time periods.

In this work it was demonstrated that slight variations in the chemistry of a poly(2-propyl-2-oxazoline) chain and the addition of further components (PLA, water/methanol mixtures) lead to unexpected phase behaviors which need careful evaluation in the exploration of new applications. It can be anticipated that the unique particle morphology of PiPOx-*b*-PLA dispersions leads to altered drug loading and release properties in comparison to PEG-*b*-PLA dispersions in which the drug is loaded into a dispersed phase consisting of PLA only. Investigations in this regard are ongoing.

References

1. Evans D. Fennell & Wennerström Håkan. *The colloidal domain*. (Wiley-VCH, 1999).
2. For the definition of the term ‘phase’ see IUPAC Gold Book (accessed 27.08.2019).
3. Szwarc, M. ‘Living’ Polymers. *Nature* **178**, 1168–1169 (1956).
4. Kagiya, T., Narisawa, S., Maeda, T. & Fukui, K. Ring-opening polymerization of 2-substituted 2-oxazolines. *J. Polym. Sci. [B]* **4**, 441–445 (1966).
5. Seeliger, W. *et al.* Recent Syntheses and Reactions of Cyclic Imidic Esters. *Angew. Chem. Int. Ed. Engl.* **5**, 875–888 (1966).
6. Tomalia, D. A. & Sheetz, D. P. Homopolymerization of 2-alkyl- and 2-aryl-2-oxazolines. *J. Polym. Sci. [A1]* **4**, 2253–2265 (1966).
7. Bassiri, T. G., Levy, A. & Litt, M. Polymerization of cyclic imino ethers. I. Oxazolines. *J. Polym. Sci. [B]* **5**, 871–879 (1967).
8. Levy, A. & Litt, M. Polymerization of cyclic imino ethers. II. Oxazines. *J. Polym. Sci. [B]* **5**, 881–886 (1967).
9. Hrkach, J. S. & Matyjaszewski, K. Reaction of 2-methyl-2-oxazoline with trimethylsilyl initiators: an unusual mode of ring opening. *Macromolecules* **25**, 2070–2075 (1992).
10. Levy, A. & Litt, M. Polymerization of cyclic iminoethers. IV. Oxazoline polymerization in solvents containing different functional groups. *J. Polym. Sci. [A1]* **6**, 63–72 (1968).
11. Verbraeken, B., Monnery, B. D., Lava, K. & Hoogenboom, R. The chemistry of poly(2-oxazoline)s. *Eur. Polym. J.* **88**, 451–469 (2017).
12. Glassner, M., Vergaelen, M. & Hoogenboom, R. Poly(2-oxazoline)s: A comprehensive overview of polymer structures and their physical properties. *Polym. Int.* **67**, 32–45 (2018).

13. Guillerm, B., Monge, S., Lapinte, V. & Robin, J.-J. How to Modulate the Chemical Structure of Polyoxazolines by Appropriate Functionalization. *Macromol. Rapid Commun.* **33**, 1600–1612 (2012).
14. Kobayashi, S., Iijima, S., Igarashi, T. & Saegusa, T. Synthesis of a nonionic polymer surfactant from cyclic imino ethers by the initiator method. *Macromolecules* **20**, 1729–1734 (1987).
15. Bloksma, M. M. *et al.* Poly(2-cyclopropyl-2-oxazoline): From Rate Acceleration by Cyclopropyl to Thermoresponsive Properties. *Macromolecules* **44**, 4057–4064 (2011).
16. Goossens, H. *et al.* Cationic Ring-Opening Polymerization of 2-Propyl-2-oxazolines: Understanding Structural Effects on Polymerization Behavior Based on Molecular Modeling. *ACS Macro Lett.* **2**, 651–654 (2013).
17. Monnery, B. D., Shaunak, S., Thanou, M. & Steinke, J. H. G. Improved Synthesis of Linear Poly(ethylenimine) via Low-Temperature Polymerization of 2-Isopropyl-2-oxazoline in Chlorobenzene. *Macromolecules* **48**, 3197–3206 (2015).
18. Aoi, K. & Okada, M. Polymerization of oxazolines. *Prog. Polym. Sci.* **21**, 151–208 (1996).
19. Lav, T.-X. *et al.* Development of a new azido-oxazoline monomer for the preparation of amphiphilic graft copolymers by combination of cationic ring-opening polymerization and click chemistry. *React. Funct. Polym.* **73**, 1001–1008 (2013).
20. Levy, A. & Litt, M. Polymerization of cyclic iminoethers. V. 1,3-oxazolines with hydroxy-, acetoxy-, and carboxymethyl-alkyl groups in the 2 position and their polymers. *J. Polym. Sci. [A1]* **6**, 1883–1894 (1968).
21. Hartlieb, M. *et al.* Cationic poly(2-oxazoline) hydrogels for reversible DNA binding. *Soft Matter* **9**, 4693–4704 (2013).
22. Flory Paul J. *Principles of Polymer Chemistry: Chapter XII*. (Cornell University Press, 1953).

23. Huggins, M. L. Some Properties of Solutions of Long-chain Compounds. *J. Phys. Chem.* **46**, 151–158 (1942).
24. Huggins, M. L. THERMODYNAMIC PROPERTIES OF SOLUTIONS OF LONG-CHAIN COMPOUNDS. *Ann. N. Y. Acad. Sci.* **43**, 1–32 (1942).
25. Huggins, M. L. Theory of Solutions of High Polymers1. *J. Am. Chem. Soc.* **64**, 1712–1719 (1942).
26. Scott, R. L. The Thermodynamics of High Polymer Solutions. V. Phase Equilibria in the Ternary System: Polymer 1—Polymer 2—Solvent. *J. Chem. Phys.* **17**, 279–284 (1949).
27. Tompa, H. Phase relationships in polymer solutions. *Trans. Faraday Soc.* **45**, 1142–1152 (1949).
28. Ulf Gedde. *Polymer Physics*. (Springer, 1999).
29. Strobl, G. *The Physics of Polymers, Chapter 4*. (Springer Berlin Heidelberg, 2007).
30. Lauritzen John I. & Hoffman John D. Theory of Formation of Polymer Crystals with Folded Chains in Dilute Solution. *J. Res. Natl. Bur. Stand. - Phys. Chem.* **64A**, 73–102 (1960).
31. Hoffman John D., Frolen Lois J., Ross Gaylon S. & Lauritzen John I. On the Growth Rate of Spherulites and Axialites from the Melt in Polyethylene Fractions: Regime I and Regime II Crystallization. *J. Res. Natl. Bur. Stand. - Phys. Chem.* **79A**, 671–699 (1975).
32. Lauritzen, J. I. Effect of a finite substrate length upon polymer crystal lamellar growth rate. *J. Appl. Phys.* **44**, 4353–4359 (1973).
33. Saeidlou, S., Huneault, M. A., Li, H. & Park, C. B. Poly(lactic acid) crystallization. *Prog. Polym. Sci.* **37**, 1657–1677 (2012).
34. Hoogenboom, R. & Schlaad, H. Thermoresponsive poly(2-oxazoline)s, polypeptoids, and polypeptides. *Polym. Chem.* **8**, 24–40 (2017).

35. Weber, C., Hoogenboom, R. & Schubert, U. S. Temperature responsive bio-compatible polymers based on poly(ethylene oxide) and poly(2-oxazoline)s. *Top. Issue Biorelated Polym.* **37**, 686–714 (2012).
36. Lin, P., Clash, C., Pearce, E. M., Kwei, T. K. & Aponte, M. A. Solubility and miscibility of poly(ethyl oxazoline). *J. Polym. Sci. Part B Polym. Phys.* **26**, 603–619 (1988).
37. Uyama, H. & Kobayashi, S. A Novel Thermo-Sensitive Polymer. Poly(2-iso-propyl-2-oxazoline). *Chem. Lett.* **21**, 1643–1646 (1992).
38. Park, J.-S. & Kataoka, K. Comprehensive and Accurate Control of Thermosensitivity of Poly(2-alkyl-2-oxazoline)s via Well-Defined Gradient or Random Copolymerization. *Macromolecules* **40**, 3599–3609 (2007).
39. Okada, Y. & Tanaka, F. Cooperative Hydration, Chain Collapse, and Flat LCST Behavior in Aqueous Poly(N-isopropylacrylamide) Solutions. *Macromolecules* **38**, 4465–4471 (2005).
40. Tanaka Fumihiko. *Polymer Physics: Applications to Molecular Association and Thermoreversible Gelation*. (Cambridge University Press, 2011).
41. Hoogenboom, R. *et al.* Tuning the LCST of poly(2-oxazoline)s by varying composition and molecular weight: alternatives to poly(N-isopropylacrylamide)? *Chem. Commun.* 5758–5760 (2008). doi:10.1039/B813140F
42. Christova, D., Velichkova, R., Loos, W., Goethals, E. J. & Prez, F. D. New thermo-responsive polymer materials based on poly(2-ethyl-2-oxazoline) segments. *Polymer* **44**, 2255–2261 (2003).
43. Diab, C., Akiyama, Y., Kataoka, K. & Winnik, F. M. Microcalorimetric Study of the Temperature-Induced Phase Separation in Aqueous Solutions of Poly(2-isopropyl-2-oxazolines). *Macromolecules* **37**, 2556–2562 (2004).
44. Zhou, Y., Tang, H. & Wu, P. Intra-molecular interactions dominating the dehydration of a poly(2-isopropyl-2-oxazoline)-based densely grafted polymer comb in aqueous

solution and hysteretic liquid-liquid phase separation. *Phys. Chem. Chem. Phys.* **19**, 6626–6635 (2017).

45. Park, J.-S. & Kataoka, K. Precise Control of Lower Critical Solution Temperature of Thermosensitive Poly(2-isopropyl-2-oxazoline) via Gradient Copolymerization with 2-Ethyl-2-oxazoline as a Hydrophilic Comonomer. *Macromolecules* **39**, 6622–6630 (2006).
46. Huber, S. & Jordan, R. Modulation of the lower critical solution temperature of 2-Alkyl-2-oxazoline copolymers. *Colloid Polym. Sci.* **286**, 395–402 (2008).
47. Kowalczuk, A., Kronek, J., Bosowska, K., Trzebicka, B. & Dworak, A. Star poly(2-ethyl-2-oxazoline)s—synthesis and thermosensitivity. *Polym. Int.* **60**, 1001–1009 (2011).
48. Jung, Y., Kim, J.-H. & Jang, W.-D. Linear and cyclic poly(2-isopropyl-2-oxazoline)s for fine control of thermoresponsiveness. *Eur. Polym. J.* **88**, 605–612 (2017).
49. Bloksma, M. M., Bakker, D. J., Weber, C., Hoogenboom, R. & Schubert, U. S. The Effect of Hofmeister Salts on the LCST Transition of Poly(2-oxazoline)s with Varying Hydrophilicity. *Macromol. Rapid Commun.* **31**, 724–728 (2010).
50. Lambermont-Thijs, H. M. L., Kuringen, H. P. C. van, Put, J. P. W. van der, Schubert, U. S. & Hoogenboom, R. Temperature Induced Solubility Transitions of Various Poly(2-oxazoline)s in Ethanol-Water Solvent Mixtures. *Polymers* **2**, (2010).
51. Schild, H. G., Muthukumar, M. & Tirrell, D. A. Cononsolvency in mixed aqueous solutions of poly(N-isopropylacrylamide). *Macromolecules* **24**, 948–952 (1991).
52. Winnik, F. M., Ringsdorf, H. & Venzmer, J. Methanol-water as a co-nonsolvent system for poly(N-isopropylacrylamide). *Macromolecules* **23**, 2415–2416 (1990).
53. Tanaka, F., Koga, T., Kojima, H., Xue, N. & Winnik, F. M. Preferential Adsorption and Co-nonsolvency of Thermoresponsive Polymers in Mixed Solvents of Water/Methanol. *Macromolecules* **44**, 2978–2989 (2011).

54. Tanaka, F., Koga, T. & Winnik, F. M. Temperature-Responsive Polymers in Mixed Solvents: Competitive Hydrogen Bonds Cause Cononsolvency. *Phys. Rev. Lett.* **101**, 028302 (2008).

55. Pica, A. & Graziano, G. An alternative explanation of the cononsolvency of poly(N-isopropylacrylamide) in water–methanol solutions. *Phys. Chem. Chem. Phys.* **18**, 25601–25608 (2016).

56. Dalgicdir, C., Rodríguez-Ropero, F. & van der Vegt, N. F. A. Computational Calorimetry of PNIPAM Cononsolvency in Water/Methanol Mixtures. *J. Phys. Chem. B* **121**, 7741–7748 (2017).

57. Rodríguez-Ropero, F., Hajari, T. & van der Vegt, N. F. A. Mechanism of Polymer Collapse in Miscible Good Solvents. *J. Phys. Chem. B* **119**, 15780–15788 (2015).

58. Mukherji, D., Marques, C. M. & Kremer, K. Polymer collapse in miscible good solvents is a generic phenomenon driven by preferential adsorption. *Nat. Commun.* **5**, 4882 (2014).

59. Mukherji, D. *et al.* Relating side chain organization of PNIPAm with its conformation in aqueous methanol. *Soft Matter* **12**, 7995–8003 (2016).

60. Bischofberger, I., Calzolari, D. C. E., De Los Rios, P., Jelezarov, I. & Trappe, V. Hydrophobic hydration of poly-N-isopropyl acrylamide: a matter of the mean energetic state of water. *Sci. Rep.* **4**, 4377 (2014).

61. Bischofberger, I., Calzolari, D. C. E. & Trappe, V. Co-nonsolvency of PNiPAM at the transition between solvation mechanisms. *Soft Matter* **10**, 8288–8295 (2014).

62. Scherzinger, C. *et al.* Cononsolvency of mono- and di-alkyl N-substituted poly(acrylamide)s and poly(vinyl caprolactam). *Polymer* **62**, 50–59 (2015).

63. Demirel, A. L., Meyer, M. & Schlaad, H. Formation of Polyamide Nanofibers by Directional Crystallization in Aqueous Solution. *Angew. Chem. Int. Ed.* **46**, 8622–8624 (2007).

64. Diehl, C. *et al.* Mechanistic study of the phase separation/crystallization process of poly(2-isopropyl-2-oxazoline) in hot water. *Soft Matter* **6**, 3784–3788 (2010).
65. Katsumoto, Y., Tsuchiizu, A., Qiu, X. & Winnik, F. M. Dissecting the Mechanism of the Heat-Induced Phase Separation and Crystallization of Poly(2-isopropyl-2-oxazoline) in Water through Vibrational Spectroscopy and Molecular Orbital Calculations. *Macromolecules* **45**, 3531–3541 (2012).
66. Demirel, A. L. *et al.* Revisiting the crystallization of poly(2-alkyl-2-oxazoline)s. *J. Polym. Sci. Part B Polym. Phys.* **54**, 721–729 (2016).
67. Furuncuoğlu Özaltın, T., Aviyente, V., Atılgan, C. & Demirel, L. Multiscale modeling of poly(2-isopropyl-2-oxazoline) chains in aqueous solution. *Eur. Polym. J.* **88**, 594–604 (2017).
68. Dai, J., Goh, S. H., Lee, S. Y. & Siow, K. S. Miscibility and interpolymer complexation of poly(2-methyl-2-oxazoline) with hydroxyl-containing polymers. *J. Polym. Res.* **2**, 209–215 (1995).
69. Kobayashi, S., Kaku, M. & Saegusa, T. Miscibility of poly(2-oxazolines) with commodity polymers. *Macromolecules* **21**, 334–338 (1988).
70. Paul, D. R. & Barlow, J. W. A binary interaction model for miscibility of copolymers in blends. *Polymer* **25**, 487–494 (1984).
71. Keskkula, H. & Paul, D. R. Miscibility of polyethyloxazoline with thermoplastic polymers. *J. Appl. Polym. Sci.* **31**, 1189–1197 (1986).
72. Aoi, K., Takasu, A. & Okada, M. New chitin-based polymer hybrids, 1. Miscibility of poly(vinyl alcohol) with chitin derivatives. *Macromol. Rapid Commun.* **16**, 757–761 (1995).
73. Aoi, K., Takasu, A., Tsuchiya, M. & Okada, M. New chitin-based polymer hybrids, 3. Miscibility of chitin-graft-poly(2-ethyl-2-oxazoline) with poly(vinyl alcohol). *Macromol. Chem. Phys.* **199**, 2805–2811 (1998).

74. Zhu, K. J., Kwei, T. K. & Pearce, E. M. Thermostability of poly(p-hydroxystyrene) blends with poly(vinyl pyrrolidone) and poly(ethyl oxazoline). *J. Appl. Polym. Sci.* **37**, 573–578 (1989).

75. Isasi, J. R., Meaurio, E., Cesteros, C. & Katime, I. Miscibility and specific interactions in blends of poly(2-ethyl-2-oxazoline) with hydroxylated polymethacrylates. *Macromol. Chem. Phys.* **197**, 641–649 (1996).

76. Lichkus, A. M., Painter, P. C. & Coleman, M. M. Hydrogen bonding in polymer blends. 5. Blends involving polymers containing methacrylic acid and oxazoline groups. *Macromolecules* **21**, 2636–2641 (1988).

77. Aoi, K., Takasu, A. & Okada, M. Miscibility of poly(vinyl chloride) with chitin derivatives having poly(2-methyl-2-oxazoline) side chains. *Macromol. Rapid Commun.* **16**, 53–58 (1995).

78. Saegusa, T. & Kobayashi, S. Oligomers Derived from 2-Oxazolines. *J. Macromol. Sci. Part - Chem.* **21**, 1021–1034 (1984).

79. Nemoto, T., Konishi, G., Tojo, Y., An, Y. C. & Funaoka, M. Functionalization of lignin: Synthesis of lignophenol-graft-poly(2-ethyl-2-oxazoline) and its application to polymer blends with commodity polymers. *J. Appl. Polym. Sci.* **123**, 2636–2642 (2012).

80. Miyamoto, M., Sano, Y., Saegusa, T. & Kobayashi, S. Synthesis of poly[(N-acylethylenimine)-b-(ethylene oxide)] and its antielectrostatic property. *Eur. Polym. J.* **19**, 955–961 (1983).

81. Sano, Y., Miyamoto, M., Kimura, Y. & Saegusa, T. N-acetylpolyethylenimine. *Polym. Bull.* **6**, 163–168 (1981).

82. Yilgor, I., Steckle Jr., W. P., Yilgor, E., Freelin, R. G. & Riffle, J. S. Novel triblock siloxane copolymers: Synthesis, characterization, and their use as surface modifying additives. *J. Polym. Sci. Part Polym. Chem.* **27**, 3673–3690 (1989).

83. Litt, M., Rahl, F. & Roldan, L. G. Polymerization of cyclic imino ethers. VI. X-ray study of some polyaziridines. *J. Polym. Sci. Part -2 Polym. Phys.* **7**, 463–473 (1969).
84. For the definition of the term ‘colloidal dispersion’ see IUPAC Gold Book (accessed 29.07.2019).
85. Hadjichristidis, N, Pispas, S & Floudas, G. *Block copolymers: Synthetic Strategies, Physical Properties, and Applications*. (John Wiley & Sons, 2003).
86. Discher, D. E. & Eisenberg, A. Polymer Vesicles. *Science* **297**, 967–973 (2002).
87. Sanson, C. *et al.* Biocompatible and Biodegradable Poly(trimethylene carbonate)-b-Poly(l-glutamic acid) Polymersomes: Size Control and Stability. *Langmuir* **26**, 2751–2760 (2010).
88. Huang, J., Bonduelle, C., Thévenot, J., Lecommandoux, S. & Heise, A. Biologically Active Polymersomes from Amphiphilic Glycopeptides. *J. Am. Chem. Soc.* **134**, 119–122 (2012).
89. Hebbeker, P., Steinschulte, A. A., Schneider, S. & Plamper, F. A. Balancing Segregation and Complexation in Amphiphilic Copolymers by Architecture and Confinement. *Langmuir* **33**, 4091–4106 (2017).
90. Synatschke, C. V. *et al.* Multicompartment Micelles with Adjustable Poly(ethylene glycol) Shell for Efficient in Vivo Photodynamic Therapy. *ACS Nano* **8**, 1161–1172 (2014).
91. Synatschke, C. V. *et al.* Micellar Interpolyelectrolyte Complexes with a Compartmentalized Shell. *Macromolecules* **46**, 6466–6474 (2013).
92. Synatschke, C. V., Schacher, F. H., Fortsch, M., Drechsler, M. & Muller, A. H. E. Double-layered micellar interpolyelectrolyte complexes-how many shells to a core? *Soft Matter* **7**, 1714–1725 (2011).
93. Wilson, P., Ke, P. C., Davis, T. P. & Kempe, K. Poly(2-oxazoline)-based micro- and nanoparticles: A review. *Eur. Polym. J.* doi:10.1016/j.eurpolymj.2016.09.011

94. Vlassi, E., Papagiannopoulos, A. & Pispas, S. Amphiphilic poly(2-oxazoline) copolymers as self-assembled carriers for drug delivery applications. *Eur. Polym. J.* **88**, 516–523 (2017).
95. Woodle, M. C., Engbers, C. M. & Zalipsky, S. New Amphipatic Polymer-Lipid Conjugates Forming Long-Circulating Reticuloendothelial System-Evading Liposomes. *Bioconjug. Chem.* **5**, 493–496 (1994).
96. Barz, M., Luxenhofer, R., Zentel, R. & Vicent, M. J. Overcoming the PEG-addiction: well-defined alternatives to PEG, from structure–property relationships to better defined therapeutics. *Polym. Chem.* **2**, 1900–1918 (2011).
97. Bauer, M. *et al.* Poly(2-ethyl-2-oxazoline) as Alternative for the Stealth Polymer Poly(ethylene glycol): Comparison of in vitro Cytotoxicity and Hemocompatibility. *Macromol. Biosci.* **12**, 986–998 (2012).
98. Knop, K., Hoogenboom, R., Fischer, D. & Schubert, U. S. Poly(ethylene glycol) in Drug Delivery: Pros and Cons as Well as Potential Alternatives. *Angew. Chem. Int. Ed.* **49**, 6288–6308 (2010).
99. Grube, M., Leiske, M. N., Schubert, U. S. & Nischang, I. POx as an Alternative to PEG? A Hydrodynamic and Light Scattering Study. *Macromolecules* **51**, 1905–1916 (2018).
100. https://clinicaltrials.gov/ct2/show/NCT02579473 (accessed 06.08.2019).
101. Moreadith, R. W. *et al.* Clinical development of a poly(2-oxazoline) (POZ) polymer therapeutic for the treatment of Parkinson's disease – Proof of concept of POZ as a versatile polymer platform for drug development in multiple therapeutic indications. *Eur. Polym. J.* **88**, 524–552 (2017).
102. Mero, A., Fang, Z., Pasut, G., Veronese, F. M. & Viegas, T. X. Selective conjugation of poly(2-ethyl 2-oxazoline) to granulocyte colony stimulating factor. *J. Controlled Release* **159**, 353–361 (2012).

103. Lee, B. K., Yun, Y. & Park, K. PLA micro- and nano-particles. *Adv. Drug Deliv. Rev.* (2016). doi:10.1016/j.addr.2016.05.020

104. Tyler, B., Gullotti, D., Mangraviti, A., Utsuki, T. & Brem, H. Polylactic acid (PLA) controlled delivery carriers for biomedical applications. *Adv. Drug Deliv. Rev.* **107**, 163–175 (2016).

105. Lee, S. C. *et al.* Synthesis and Micellar Characterization of Amphiphilic Diblock Copolymers Based on Poly(2-ethyl-2-oxazoline) and Aliphatic Polyesters1. *Macromolecules* **32**, 1847–1852 (1999).

106. Wang, C.-H. & Hsiue, G.-H. New Amphiphilic Poly(2-ethyl-2-oxazoline)/ Poly(l-lactide) Triblock Copolymers. *Biomacromolecules* **4**, 1487–1490 (2003).

107. Hsiue, G.-H. *et al.* Environmental-sensitive micelles based on poly(2-ethyl-2-oxazoline)-b-poly(l-lactide) diblock copolymer for application in drug delivery. *Int. J. Pharm.* **317**, 69–75 (2006).

108. Wang, C.-H., Wang, C.-H. & Hsiue, G.-H. Polymeric micelles with a pH-responsive structure as intracellular drug carriers. *J. Controlled Release* **108**, 140–149 (2005).

109. Su, F. *et al.* Novel self-assembled micelles of amphiphilic poly(2-ethyl-2-oxazoline) - poly(L-lactide) diblock copolymers for sustained drug delivery. *Colloids Surf. Physicochem. Eng. Asp.* **566**, 120–127 (2019).

110. Zhao, Y. *et al.* pH-responsive polymeric micelles based on poly(2-ethyl-2-oxazoline)-poly(d,l-lactide) for tumor-targeting and controlled delivery of doxorubicin and P-glycoprotein inhibitor. *Acta Biomater.* **17**, 182–192 (2015).

111. Le Fer, G., Le Cœur, C., Guigner, J.-M., Amiel, C. & Volet, G. Amphiphilic diblock and triblock copolymers based on poly(2-methyl-2-oxazoline) and poly(D,L-lactide): Synthesis, physicochemical characterizations and self-assembly properties. *Polymer* **171**, 149–160 (2019).

112. Shieh, M.-J. *et al.* Reduced Skin Photosensitivity with meta-Tetra(hydroxyphenyl)chlorin-Loaded Micelles Based on a Poly(2-ethyl-2-oxazoline)-b-poly(d,l-lactide) Diblock Copolymer in Vivo. *Mol. Pharm.* **7**, 1244–1253 (2010).
113. Park, J.-S., Akiyama, Y., Yamasaki, Y. & Kataoka, K. Preparation and Characterization of Polyion Complex Micelles with a Novel Thermosensitive Poly(2-isopropyl-2-oxazoline) Shell via the Complexation of Oppositely Charged Block Ionomers. *Langmuir* **23**, 138–146 (2007).
114. Witte, H. & Seeliger, W. Cyclische Imidsäureester aus Nitrilen und Aminoalkoholen. *Justus Liebigs Ann. Chem.* **1974**, 996–1009 (1974).
115. Fedors, R. F. A method for estimating both the solubility parameters and molar volumes of liquids. *Polym. Eng. Sci.* **14**, 147–154 (1974).
116. Kowalewski, V. J. & de Kowalewski, D. G. Proton NMR Spectra of the N,N-Dimethylformamide, N-Methylformamide, and N,N-Dimethylacetamide. *J. Chem. Phys.* **32**, 1272–1273 (1960).
117. Leibler, L. Theory of Microphase Separation in Block Copolymers. *Macromolecules* **13**, 1602–1617 (1980).
118. Kaplan, D. S. Structure–property relationships in copolymers to composites: Molecular interpretation of the glass transition phenomenon. *J. Appl. Polym. Sci.* **20**, 2615–2629 (1976).
119. Pan, P., Kai, W., Zhu, B., Dong, T. & Inoue, Y. Polymorphous Crystallization and Multiple Melting Behavior of Poly(l-lactide): Molecular Weight Dependence. *Macromolecules* **40**, 6898–6905 (2007).
120. Sun, S. & Wu, P. Conformational changes in the heat-induced crystallization of poly(2-isopropyl-2-oxazoline) in the solid state. *Phys. Chem. Chem. Phys.* **17**, 31084–31092 (2015).
121. De Santis, P. & Kovacs, A. J. Molecular conformation of poly(S-lactic acid). *Biopolymers* **6**, 299–306 (1968).

122. Heald, C. R. *et al.* Poly(lactic acid)−Poly(ethylene oxide) (PLA−PEG) Nanoparticles: NMR Studies of the Central Solidlike PLA Core and the Liquid PEG Corona. *Langmuir* **18**, 3669–3675 (2002).
123. Pagels, R. F., Edelstein, J., Tang, C. & Prud'homme, R. K. Controlling and Predicting Nanoparticle Formation by Block Copolymer Directed Rapid Precipitations. *Nano Lett.* **18**, 1139–1144 (2018).
124. Mössmer, S. *et al.* Solution Behavior of Poly(styrene)-block-poly(2-vinylpyridine) Micelles Containing Gold Nanoparticles. *Macromolecules* **33**, 4791–4798 (2000).
125. Allegra, G. & Ganazzoli, F. Polymer collapse in dilute solution: Equilibrium and dynamical aspects. *J. Chem. Phys.* **83**, 397–412 (1985).

I Pooch, F.; Teltevskij, V.; Karjalainen, E.; Tenhu, H.; Winnik, F. M. **Poly(2-propyl-2-oxazoline)s in aqueous methanol: to dissolve or not to dissolve….** *Macromolecules*, **2019,** *52,* 6361-6368. DOI: 10.1021/acs.macromol.9b01234

II Pooch, F.; Sliepen, M.; Svedström, K. J.; Korpi, A.; Winnik, F. M.; Tenhu, H. **Inversion of crystallization rates in miscible block copolymers of poly(lactide)-*block*-poly(2-isopropyl-2-oxazoline).** *Polymer Chemistry* **2018**, *9*, 1848-1856. DOI: 10.1039/c8py00198g

III Pooch, F.; Sliepen, M.; Knudsen, K. D.; Nyström, B.; Tenhu, H.; Winnik, F. M. **Poly(2-isopropyl-2-oxazoline)-*b*-poly(lactide) (PiPOx-*b*-PLA) Nanoparticles in Water: Interblock van der Waals Attraction Opposes Amphiphilic Phase Separation.** *Macromolecules* **2019**, *52*, 1317-1326. DOI: 10.1021/acs.macromol.8b02558